Exploration of individual colorectal cancer cell responses to H_2O_2 eustress using hopping probe scanning ion conductance microscopy

Dong Wang[1], Emily Woodcock[2,3], Xi Yang[1], Hiromi Nishikawa[1], Elena V Sviderskaya[3], Masanobu Oshima[1], Christopher Edwards[2], Yanjun Zhang[1,2,*] , Yuri Korchev[2,1,*]

[1]WPI Nano Life Science Institute (WPI–Nano LSI), Kanazawa University, Kanazawa 920–1192, Japan;
[2]Department of Medicine, Imperial College London, London W12 0NN, United Kingdom;
[3]Cell Biology Research Centre, Molecular and Clinical Sciences Research Institute, St George's, University of London, London SW17 0RE, United Kingdom.

***Corresponding authors**: yanjunzhang@staff.kanazawa–u.ac.jp, y.korchev@imperial.ac.uk

Keywords: SPM, Nanoprobe, Nanobiology, SECM, ROS, Stiffness

Abstract

Colorectal cancer (CRC), a widespread malignancy, is closely associated with tumor microenvironmental hydrogen peroxide (H_2O_2) levels. Some clinical trials targeting H_2O_2 for cancer treatment have revealed its paradoxical role as a promoter of cancer progression. Investigating the dynamics of cancer cell H_2O_2 eustress at the single–cell level is crucial. In this study, non–contact hopping probe mode scanning ion conductance microscopy (HPICM) with high−sensitive Pt–functionalized nanoelectrodes was employed to measure dynamic extracellular to intracellular H_2O_2 gradients in individual colorectal cancer Caco–2 cells. We explored the relationship between cellular mechanical properties and H_2O_2 gradients. Exposure to 0.1 or 1 mmol/L H_2O_2 eustress increased the extracellular to intracellular H_2O_2 gradient from 0.3 to 1.91 or 3.04, respectively. Notably, cellular F–actin–dependent stiffness increased at 0.1 mmol/L but decreased at 1 mmol/L H_2O_2 eustress. This H_2O_2–induced stiffness modulated AKT activation positively and GPX2 expression negatively. Our findings unveil the failure of some H_2O_2–targeted therapies due to their ineffectiveness in generating H_2O_2, which instead acts eustress to promote cancer cell survival. This research also reveals the complex interplay between physical properties and biochemical signaling in cancer cells' antioxidant defense, illuminating the exploitation of H_2O_2 eustress for survival at the single–cell level. Inhibiting GPX and/or CAT enhances the cytotoxic activity of H_2O_2 eustress against CRC cells, which holds significant promise for developing innovative therapies targeting cancer and other H_2O_2–related inflammatory diseases.

1. Introduction

Colorectal cancer (CRC) is one of the most common malignant tumors worldwide. Its development is not only controlled by genetic and epigenetic regulation but is also closely related to the tumor microenvironment [1]. Notably, CRC is among the few solid tumors where reactive oxygen species (ROS), a mediator of inflammation, plays a pivotal role in the mechanism of carcinogenesis, transforming normal cells into malignant ones [2, 3]. The major and stable ROS derivative, hydrogen peroxide (H_2O_2), exhibits a dual role as a eustressor in cellular signaling functions; however, at supraphysiological concentrations, it induces cytotoxicity [3-5]. This unique characteristic presents a promising avenue for exploiting H_2O_2 in cancer treatment, particularly in combination with radiotherapy and chemotherapy [6]. Despite recent studies revealing the importance of H_2O_2 regulation in cancer cells, the specific mechanisms required to dynamically fine–tune the delicate balance in local H_2O_2 levels remain elusive [7, 8]. Moreover, many H_2O_2 regulation clinical trials have not only failed to reduce but have actually promoted cancer progression. This suggests that cancer cells may deliberately maintain H_2O_2 levels as eustress (i.e. beneficial stress), and more research targeting defined H_2O_2 mechanisms is clearly needed [3].

Accumulating evidence highlights the significant role of cell stiffness in regulating cancer cell functions, metastatic preferences, and their response to H_2O_2 [9, 10]. Although the polymerization–depolymerization dynamics of the actin cytoskeleton have been identified as targets for H_2O_2 and can influence cell stiffness, the precise mechanisms governing this relationship remain incompletely understood [2, 11]. In recent years, non–contact hopping probe mode of scanning ion conductance microscopy (HPICM) has emerged as a powerful technique to explore the nanomechanical properties of living cells [12-14]. Unlike atomic force microscopy (AFM), which relies on direct contact with the cell membrane and may cause damage during scanning [15], HPICM enables repetitive investigation of mechanical changes in the same cell without disrupting its cellular structures [13, 14]. By utilizing HPICM, our study aims to unravel the intricate mechanisms underlying the interplay between the mechanical properties of individual cancer cells and their response to H_2O_2.

The distribution of H_2O_2 gradients across cell membranes plays a crucial role in H_2O_2 signaling, similar to the significance of pH and calcium gradients in cellular signaling [3, 16]. To gain insights into H_2O_2 signaling mechanisms, it is necessary to characterize the ratio between extracellular and intracellular H_2O_2 concentrations, which defines the H_2O_2 gradient [8, 17]. However, existing methods for gradient evaluation often involve experimental quantification of extracellular H_2O_2, followed by theoretical estimation of intracellular H_2O_2 levels, or vice versa [18, 19]. Moreover, conventional H_2O_2 detection methods, such as fluorescent probes, suffer from challenges like rapid off−site diffusion, photo–bleaching, and irreversibility, hampering continuous spatiotemporal monitoring of H_2O_2 from the same cell [20]. Genetically encoded biosensors like Hyper or RoGFP offer cellular H_2O_2 quantification, but their limited working range and the necessity for genetic manipulation of cells restrict their broader application [16].

Furthermore, H_2O_2 measurements from cell populations may mask vital cellular differences, highlighting the need for new strategies to detect H_2O_2 at the single–cell level [3]. Electrochemical H_2O_2 sensors, particularly those employing platinum (Pt) nanoelectrodes, provide a rapid response, have high sensitivity, and excellent anti–interference properties for accurate quantification of H_2O_2 levels in biological systems [21, 22]. Moreover, Pt–functionalized nanoelectrodes operating at + 0.45 V have been demonstrated to exhibit enhanced selectivity for H_2O_2 detection [23]. By combining high spatial resolution HPICM with highly–selective Pt–functionalized nanoelectrodes, real–time monitoring of extracellular and intracellular H_2O_2 concentrations has become possible, offering valuable insights into H_2O_2–mediated processes at the single–cell level [21]. In this study, we aim to characterize and quantify cellular H_2O_2 gradients, enabling specific probing of H_2O_2 levels and distinguishing individual cellular responses from the bulk environment.

Caco–2 cells, derived from human colorectal adenocarcinoma intestinal epithelial cells, offer a valuable *in vitro* model for studying H_2O_2 signaling in cancer progression [24]. Leveraging the combined HPICM and Pt–functionalized nanoelectrodes, our study aims to explore the cell mechanics and H_2O_2 response of individual Caco–2 cells at the single–cell level. The findings from this investigation provide valuable insights into the intricate interplay between H_2O_2–induced changes in physical properties and biochemical signaling in cancer cells, potentially guiding the development of novel H_2O_2–targeting therapeutic strategies.

2. Materials and methods

2.1. Chemicals

Phosphate buffered saline (PBS) (composed of (mmol/L)): 10 Na_2HPO_4, 2.7 KCl, 1.8 KH_2PO_4, and 137 NaCl, pH = 7.4) was prepared by dissolving tablets (2g; Sigma−Aldrich) in 200 mL deionized water (Milli–Q; Millipore Corp.). Ferrocenemethanol (FcMeOH, 98%; Sigma–Aldrich). HBSS (+) (FUJIFILM Wako Pure Chemical Corporation, Japan) composed of (mmol/L): 137.9 NaCl, 5.3 KCl, 1.3 $CaCl_2$, 0.5 $MgCl_2$, 0.34 Na_2HPO_4, 4.2 $NaHCO_3$, 0.4 $MgSO_4$, 0.5 $MgCl_2$, 0.44 KH_2PO_3, and 5.6 Glucose. pH = 7.4 at room temperature).

2.2. Cell culture

Caco–2 cells were purchased from American Type Culture Collection (ATCC) (Japanese Collection of Research Bioresources Cell Bank, Tokyo, Japan). Cells were cultured in Dulbecco's modified Eagle's medium (DMEM; Invitrogen, Carlsbad, USA) supplemented with 10% fetal bovine serum (FBS; Invitrogen, Carlsbad, USA), 2 mmol/L L–glutamine (Invitrogen, Carlsbad, CA, USA), 1% non−essential amino acids, and 1% penicillin−streptomycin (Invitrogen, Carlsbad, CA, USA). Confluent cells were trypsinized using 0.25% Trypsin–EDTA solution (Thermo Fisher Scientific, Waltham, MA, USA).

2.3. Inhibitors and activators

To investigate the real role of AMPK and AKT in the regulation of H_2O_2 eustress, we employed AMPK inhibition with 10 μmol/L Dorsomorphin 2HCl (BML–275, Compound C, Selleck Chemicals, USA) and AKT inhibition with 10 μmol/L AKTi–1/2 (ab142088, Abcam) in Caco−2 cells. To activate or inhibit the polymerization of F–actin cytoskeleton, cells were treated with 100 nmol/L jasplakinolide (Jas, Sigma–Aldrich) [25], an enhancer of F−actin cytoskeleton, or 10

μmol/L cytochalasin D (CD, Sigma–Aldrich) [13], a disruptor of F−actin cytoskeleton, for a duration of 2 hours (h).

2.4. H_2O_2 eustress levels determination to Caco−2 Cells

To optimize the concentration of H_2O_2, Caco–2 cells were seeded at a density of 1×10^6 cells/cm^2 into 35 mm petri dish or 6–wells membrane filter inserts. After cultured for 3 days, the oxidation was induced by exposing the cells to 2 h of different concentrations of H_2O_2 (0, 0.01, 0.1, 1, 10 mmol/L) in DMEM. This time–concentration combination was chosen as the acute eustress because the intention of this study was to determine the cellular responses at stressed conditions without inducing cell death.

2.5. Protein preparation and western blot analysis

Caco–2 cells were treated with 0.1 or 1 mmol/L H_2O_2 or left untreated for 2 h and subsequently were lysed with TNE solution (10 mmol/L Tris·HCl [pH 7.6], 150 mmol/L NaCl, 1 mmol/L ethylenediaminetetraacetic acid, 1% Nonidet P–40, protease inhibitor [Roche], and phosphatase inhibitor [Wako]). After sonication and centrifugation, the supernatant was mixed with 5 × sodium dodecyl sulfate sample buffer and boiled for 10 minutes (min) at 98 °C. Protein samples were separated in SDS–polyacrylamide gel. The antibodies used are shown below: Cleaved caspase−3 (Asp175) (Cell Signaling), p−AKT (S473) (Cell Signaling), p65 NFκB (Cell Signaling), p38 MAPK (Cell Signaling), HSP27 (Cell Signaling), Noxo1 (Acris), NRF2 (Cell Signaling), PFKP (Cell Signaling), p–AMPK (Cell Signaling), p−STAT3 (Cell Signaling), Catalase (Cell Signaling), GPX2 (abcam), GPX4 (Cell Signaling), PRDX1 (Cell Signaling), p53 (Cell Signaling), and an anti−GAPDH antibody was used as the internal control. Secondary antibody was applied (1 : 10000) for 1 h at room temperature. The ECL detection system (GE Healthcare) was used to detect the signals. Band intensities were measured using ImageJ application.

2.6. Transepithelial electrical resistance (TEER) measurements

TEER measurements of Caco−2 cell monolayer were investigated by a commercial epithelial volt ohmmeter (EVOM, World Precision Instruments, USA) and an ENDOHM–24 SNAP Chamber (World Precision Instruments, USA) as per previously published methods [26]. In brief, Caco–2 grown on inserts at a density of approximately 1×10^5 cells/cm^2. The culture medium is refreshed every 24−48 h. TEER studies were carried out on fully differentiated cells after 18−21 days culture. TEER measurements were performed in the HBSS (+) medium at 37 °C after the EVOM reading became stable (~30 min). TEER values are represented in the real value of Ω cm^2. Caco–2 grown on inserts with a stable initial TEER value greater than 1000 Ωcm^2 (6 wells filter insert with a surface area of 4.2 cm^2) were chosen for the experiments. TEER studies are usually done after 18–21 days in culture. TEER of unseeded inserts was just about neglectable 10 Ωcm^2.

2.7. Fabrication of the hopping probe mode scanning ion conductance microscopy (HPICM) scanning and mechanical properties measuring glass nanopipettes

HPICM scanning and mechanical properties measuring glass nanopipettes were fabricated by pulling borosilicate glass capillaries (inner diameter = 0.58 mm, outer diameter = 1.00 mm) to nanopipettes with a tip diameter of ~100 nm using a CO_2 laser puller (Model P–2000, Sutter Instruments Co., USA) [13, 27]. Nanopipettes were pulled with a two−step protocol. Briefly, for the initial step, the parameters were: heat 350, filament 3, velocity 30 and delay 200. For the

second step, they were: heat 350, filament 2, velocity 27, delay 160 and pull 250. Nanopipettes with resistance of approximately 100 MΩ filled with phosphate–buffered saline were used unless stated otherwise. The approximately 100 nm diameters of HPICM scanning nanopipettes were characterized using scanning electron microscopy (SEM), as illustrated in the supplementary information Fig. S3 (online).

2.8. HPICM scanning and mechanical property measuring protocol

HPICM scanning and mechanical properties measurements were performed using a customized HPICM setup and operated in adaptive resolution hopping probe mode using an ICAPPIC Controller (IC−UN–001, ICAPPIC Ltd, UK) as previously described [13, 14, 27]. Briefly, the HPICM scan head consisted of a PIHera P–621.2 XY Nanopositioning Stage (Physik Instrumente, Germany) with 100 × 100 μm travel range that moved the sample and a LISA piezo actuator P−753.21 C (Physik Instrumente, Germany) with travel range 25 μm for pipette positioning along the Z−axis. HPICM mounted on an inverted optical microscope Eclipse Ti–2 (Nikon, Japan) and covered by Faraday cage for electrical noise shielding. All HPICM control, data acquisition, and analysis software were written and kindly provided by Dr Pavel Novak, ICAPPIC Ltd. Ion currents were monitored using a MultiClamp 700B amplifier (Molecular Devices, USA) using a 2 kHz low–pass filter. A typical external holding voltage of 200 mV was supplied to the scanning nanopipette. During HPICM scanning and cellular stiffness mapping, the nanopipette approach rate was set at 200 μm/s, and the final images were interpolated to 256 × 256 pixels. For all HPICM morphology and mechanical property measurements, a three−set point protocol was used. A non−contact topographic image was collected at an ion current decrease of 0.5% and a further two images were collected at ion current decrease of 1% and 2% corresponding to the cell membrane deformations produced by intrinsic force of the scanning nanopipette. On the basis of the membrane deformation data obtained at each setpoint, the membrane displacement and Young's modulus were calculated using the previously described theoretical model [13].

2.9. The fabrication of Pt–functionalized carbon H_2O_2 sensing nanoprobe

Single–barrel quartz capillaries (1.0 mm o.d., 0.7 mm i.d, Intracell) were cleaned in SEDE−P soft plasma etching device (Meiwafosis, Japan) for 30 min to remove surface contaminants. The cleaned capillaries were pulled by a P–2000 laser puller (Sutter Instruments) using a custom two−line program (First line; Heat: 800, Filament: 4, Velocity: 30, Delay: 170, Pull: 80. Second–line Heat: 825, Filament: 3, Velocity: 20, Delay: 145, Pull: 130). Carbon was then deposited onto the inner wall by chemical vapor deposition using methane as carbon source and argon as protector. The size and geometry of the carbon nanoelectrodes were determined through electrochemical measurements conducted in 1 mmol/L ferrocene methanol (FcMeOH), which gives good insight into characteristic geometry as previously published method [22]. Briefly, the carbon nanoelectrode radius (r) was estimated from the steady–state current (I_{ss}) at 0.4 V in 1 mmol/L FcMeOH using the formula $I_{ss} = 4.64 \cdot r \cdot F \cdot c \cdot D$, with F as the Faraday constant, c as the concentration, and D as the diffusion coefficient (7.8×10^{-6} cm^2 s^{-1} for FcMeOH). All carbon nanoelectrodes demonstrated an estimated diameter of approximately 100 nm. Carbon nanoprobes were further electrochemical etched as previously published methods [22]. Briefly, electrochemical etching of a cavity in carbon layer was performed by cyclic voltammetry from 0 to 2.2 V in 0.1 mol/L KOH, 10 mmol/L KCl for about 15 cycles. Then electrochemical deposition of Pt was achieved by sweeping the potential from 0 V to − 0.8 V with a scan rate of 200 mV s^{-1} for 4–5 cycles in 2 mmol/L chloroplatinic acid (H_2PtCl_6, Sigma) in 0.1 mol/L

hydrochloric acid. The approximately 100 nm diameters of Pt−functionalized carbon nanoelectrodes were further validated using SEM, as illustrated in the supplementary information Fig. S5 (online).

2.10. Extracellular to intracellular H_2O_2 gradient measurement with Pt–functionalized carbon nanoelectrode

The extracellular and intracellular H_2O_2 level was measured with Pt–functionalized carbon nanoelectrode with a previously published protocol [21]. Briefly, a two–electrode setup was mounted in a 35–mm petri dish, with a platinized carbon nanoelectrode back contacted with a silver wire serving as a working electrode, and the second Ag/AgCl wire was placed in a bulk solution acting as a reference electrode. All potentials are quoted against this reference electrode. The Faradaic current was measured with a MultiClamp700B patch clamp amplifier (Molecular Devices). The electrochemical signal was filtered using a low–pass filter at 1 kHz and digitized with an Axon Digidata 1550B (Molecular Devices), and a PC equipped with pClamp 10 software (Molecular Devices). The platinized carbon nanoelectrodes were employed for less–invasive single cancer cell membrane penetration to measure extracellular and intracellular H_2O_2 concentration. To avoid tip crashing, the whole process was feedback controlled with ICAPPIC Controller (IC–UN–001, ICAPPIC Ltd, UK) and the tip position was also monitored with an inverted microscope.

Prior to each H_2O_2 sensing experiment, the Pt–functionalized carbon nanoprobe was calibrated by constructing standard curves using known H_2O_2 concentrations in HBSS (+) medium. Changes in the responses of the nanoelectrode upon exposure to H_2O_2 were quantified by the currents recorded at 2 Hz on + 0.45 V *vs*. Ag/AgCl electrode. As shown in Fig. S6a (online), the calibration standard curve of nanoelectrodes displayed a good linearity. Caco–2 cells grown on a Petri dish were kept in HBSS (+) solution at room temperature. During the detection of H_2O_2 gradients, the nanoelectrodes were positioned vertically near the surface of living cells and subsequently penetrated the cell membrane under the feedback control of HPICM, functioning as Scanning Electrochemical Microscopy. This allowed for the simultaneous measurement of extracellular and intracellular anodic currents representing H_2O_2 levels at distinct positions within the same cell. The H_2O_2 concentration was determined by converting the recorded electrical currents using a calibration curve. By calculating the ratio between extracellular and intracellular H_2O_2 levels, we were able to evaluate changes in H_2O_2 gradients in a ratio–metric manner. This approach minimized the influence of varying cell culture conditions, such as cell density and size, on the local H_2O_2 concentration, facilitating a more precise assessment of the gradients.

2.11. Extracellular H_2O_2 removal Amplex Red assay

To examine the kinetics of extracellular H_2O_2 reduction in Caco–2 cells, an Amplex Red Hydrogen Peroxide/Peroxidase Assay Kit (Invitrogen, USA) was used in accordance with the procedure described in production operations manual and previous publication [28]. To monitor the H_2O_2 concentration, Cells were grown for 72 h in the 35 mm petri dish, washed with 2 mL of HBSS (+), and H_2O_2 was added to the dish at a final concentration at the concentration of 0.1 or 1 mmol/L. Then a 1 h continuous experiment was carried out after H_2O_2 was added to the Caco–2 cells culture dish, and the changing in extracellular H_2O_2 concentrations were recorded at 1, 5, 10, and up to 60 min following treatment (with 5 min increments). An H_2O_2 standard curve was

conducted following each experiment by addition of known concentrations of H_2O_2, allowing for conversion of relative fluorescence units to H_2O_2 concentration.

2.12. FACS analysis for cell apoptosis

Cells were seeded in triplicate in 6–well plates at 5×10^5 cells / well, and allowed to grow for 72 h. The catalase inhibitor 3–aminotriazole (3AT) was obtained from Sigma–Aldrich. '3AT–treated cells' cultivated with 10 mmol/L 3AT for 24 h. 'Tiop–treated cells' cultivated with Tiopronin (Combi–Blocks Inc., 0.5 mmol/L) for 24 h. Cells were harvested, washed with PBS, then double–stained with propidium iodide (PI) and Annexin V–FITC early apoptosis detection kit (Cell Signaling Technology) for flow cytometry analysis. All samples were analyzed using flow cytometry (FACS Canto II, BD).

2.13. Actin filament labeling

Cells were exposed for 2 h to different concentrations of H_2O_2. After exposure, the cells cultured on the dish were fixed, stained for F–actin with DyLight 594 phalloidin (Cell Signaling), and fluorescent images obtained using a TCS SP8 confocal microscope (Leica Microsystems, Wetzlar, Germany). DAPI was used for counter nuclear staining.

2.14. Fluorescent immunohistochemistry

Antibodies against E–cadherin (R&D Systems) at 1 : 100, p65 NFκB (Cell Signaling) at 1 : 100, were used as the primary antibody. Alexa Fluor 594– or Alexa Fluor 488–conjugated antibodies (Molecular Probes) were used as the secondary antibody. Fluorescent images were obtained using a TCS SP8 confocal microscope (Leica Microsystems, Wetzlar, Germany). DAPI was used for counter nuclear staining.

2.15. Scanning electron microscopy (SEM) Imaging

SEM imaging utilized a Dual Beam Focused Ion Beam System (Helios G4 CX, Thermo Fisher Scientific) with accelerating voltages set at 1 or 5 kV. Further details on setup parameters can be found alongside the SEM image.

3. Results

3.1. Determination of acute exogenous H_2O_2 eustress levels in colorectal cancer Caco–2 cells

Healthy Caco–2 cells can differentiate into a polarized monolayer resembling intestinal epithelia barrier during cell culture [29]. HPICM scanning revealed that the Caco–2 cell monolayer exhibited a brush border and microvilli (Fig. 1a), which were consistent with previously observed epithelial structures from Caco–2 cells with Scanning Electron Microscopy [30]. To assess the effects of acute exogenous H_2O_2 stress on the integrity of the Caco–2 cell monolayer, transepithelial electrical resistance (TEER) measurements [26] were conducted following exposure to varying levels of H_2O_2 from 0 to 10 mmol/L for a duration of 2 h (Fig. 1b). Results showed that, as assessed by TEER, only exposure to higher concentrations of H_2O_2 (10 mmol/L) produced a significant decrease, indicating a disruption of monolayer integrity. Additionally, continuous HPICM scanning demonstrated that exposure to 1 mmol/L H_2O_2 for 2 h did not cause any observable damage to the Caco–2 cell monolayer (Fig. S1 (online)). Furthermore, healthy cell growth occurred and the cells formed a tight monolayer under 0.1 mmol/L H_2O_2 stress (Fig. S2 (online)). Flow cytometric analysis of Annexin V/PI early apoptosis detection was also performed on these H_2O_2–treated Caco–2 cells (Fig. 1c). Consistent with the results of our TEER measurements, only the highest concentration of H_2O_2 (10 mmol/L) significantly increased apoptosis. To further confirm that 0.1 mmol/L and 1 mmol/L induces eustress to cells, E–cadherin, which connects with the F–actin cytoskeleton to maintain cell–cell junctional integrity in epithelia [2], was examined by immunostaining and showed no significant changes in Caco–2 cell monolayer under 0.1 and 1 mmol/L H_2O_2 stress (Fig. S4 (online)). The Caco–2 cells survived well during the 2 h exposure to H_2O_2 concentrations up to 1 mmol/L, and hence these conditions were deemed suitable for the term "H_2O_2 eustress" on cells [3]. Therefore, in this study, acute exogenous eustress was induced in individual Caco–2 cells by subjecting them to a 2 h extracellular exposure of two intermediate concentrations of H_2O_2, namely 0.1 mmol/L and 1 mmol/L.

3.2. Investigation of extracellular to intracellular H_2O_2 gradient responses of individual Caco–2 cells to H_2O_2 eustress with HPICM combined Pt–functionalized carbon nanoelectrodes

Cellular H_2O_2 eustress should be tightly regulated in terms of its source, location, duration, and amount, as it plays a crucial role in important cellular signaling processes [5, 8]. When cells are exposed to H_2O_2, extracellular to intracellular gradients are established depending on the intensity of intracellular H_2O_2 consumption and the permeability characteristics of the cell membranes [31]. To accurately quantify H_2O_2 gradients, we utilized HPICM–controlled Pt–functionalized carbon nanoelectrodes to measure the dynamic changes in H_2O_2 gradients of individual Caco–2 cells under 0.1 and 1 mmol/L H_2O_2 eustress (Fig. 2a). The H_2O_2 calibration curve demonstrated the linear response of Pt–functionalized nanoelectrodes to H_2O_2 at 0.45 V (Fig. S6a (online)). Consistent with our previous findings in melanoma cells [21], two repetitive recordings using Pt–functionalized nanoelectrodes showed that the baseline intracellular H_2O_2 level was higher than extracellular in control Caco–2 cells (Fig. S6b (online)). Upon exposure to H_2O_2 eustress, a steeper elevation of the H_2O_2 gradient was observed, with a higher ratio of extracellular to intracellular H_2O_2 across the Caco–2 cell membrane (Fig. S6c (online)). The

statistical histogram demonstrated that the average ratio–metric extracellular to intracellular H_2O_2 gradients increased from 0.3 ± 0.13 (n = 77, control) to 1.91 ± 0.54 (n = 77, 0.1 mmol/L) and 3.04 ± 1.58 (n = 61, 1 mmol/L) (Fig. 2a).

3.3. Exploring the antioxidant defense capacities of Caco–2 cells in responding to H_2O_2 eustress

Cancer cells employ various H_2O_2 scavenging enzymes, including catalase (CAT), peroxiredoxin (PRDX), and glutathione peroxidase (GPX), to maintain redox homeostasis [4, 8, 32]. GPX2, which is specifically expressed in gastrointestinal tract epithelial cells, is known for its efficient reduction of H_2O_2 to water [33]. To understand the roles of these antioxidant enzymes in maintaining H_2O_2 gradients, the expressions of two major H_2O_2 scavenging enzymes, GPX2 and CAT (Fig. 2b), and the expression of other antioxidant enzymes, GPX4 and PRDX1 (Fig. S7 (online)), were observed in Caco–2 cells through Western blotting. Compared to the control group, the expression of GPX2 was decreased in the 0.1 mmol/L H_2O_2–treated group but then recovered in the 1 mmol/L H_2O_2–treated group. The expressions of CAT, PRDX1, and GPX4 did not exhibit dose dependency in response to H_2O_2 eustress. These results imply that GPX2 may play a more important role in fine–tuning H_2O_2 gradients and cellular functions, while CAT, PRDX1, and GPX4 may act as gatekeepers for global H_2O_2 scavenging in Caco–2 cells. Furthermore, we evaluated the defense capacities of Caco–2 cells against H_2O_2 eustress by using the Amplex Red Hydrogen Peroxide/Peroxidase Assay, following a previously published procedure [28]. Our results demonstrated the rapid elimination of extracellularly added H_2O_2 by Caco–2 cells (Fig. S8 (online)), which may be attributed to the high levels of expression of H_2O_2 scavenging enzymes observed in Caco–2 cells.

3.4. Investigation of the mechanical properties response of individual Caco–2 cells to H_2O_2 eustress with HPICM

Cell stiffness, a fundamental mechanical property, is influenced by the F–actin cytoskeleton and plays a crucial role in establishing a polarized tight epithelial monolayer [9, 10]. Using HPICM and Pt–functionalized carbon nanoelectrodes, we have previously demonstrated that anticancer treatments with docetaxel and cisplatin can increase both cellular H_2O_2 levels and stiffness in cancer cells [22]. H_2O_2 is known to induce actin polymerization [2], and higher levels of F–actin polymerization have been associated with increased cell stiffness, while a depolymerization in F–actin correlates with decreased cell stiffness [13, 34]. F–actin specific phalloidin staining was performed in a Caco–2 cell monolayer under H_2O_2 eustress by confocal microscopy imaging (Fig. S9 (online)). Compared to the control Caco–2 cell monolayer, the F–actin intensity was increased in the 0.1 mmol/L H_2O_2–treated cells, but decreased in 1 mmol/L H_2O_2–treated cells. We further used repetitive HPICM scanning and Young's modulus evaluations to investigate the involvement of cellular stiffness in individual Caco–2 cells in their response to H_2O_2 eustress at the single–cell level (Fig. 3a). We demonstrated that the cellular stiffness was higher at 0.1 mmol/L but lower at 1.0 mmol/L H_2O_2 eustress. Normalized cellular elasticity analysis within the marked region in these time–lapse HPICM scans demonstrated the dose–dependent effects of H_2O_2 eustress on cellular stiffness (Fig. 3b). Statistical analysis of a larger number of Caco–2 cells revealed that their average Young's modulus increased from 1.64 ± 0.60 kPa for control cells to 1.93 ± 0.66 kPa for 0.1 mmol/L H_2O_2–treated cells but decreased to 0.9 ± 0.41 kPa for 1

mmol/L H_2O_2–treated cells (Fig. 3c). Furthermore, the association of H_2O_2–induced cellular stiffness with actin reorganization was also investigated by actin–specific phalloidin staining at the single Caco–2 cell level (Fig. 3d). Such H_2O_2 eustress of the induced F–actin dependent stiffness changes in Caco–2 cells is in line with previous findings from another group, who also demonstrated F–actin dependent stiffness changes in fibroblasts using AFM [34].

3.5. Exploring the underlying signaling pathways of Caco–2 cells in homeodynamical responding to H_2O_2 eustress

In our study, western blotting results revealed that H_2O_2 eustress dose–dependently upregulated the expression of several signaling proteins, including p53, p−STAT3, HSP27, NRF2, p38–MAPK, NOXO1, PFKP, and NFκB (Fig. S10a (online)). All these proteins and signaling pathways have been previously demonstrated to be activated by oxidative stress, suggesting that our Caco–2 cell model reflects the general phenomenon of H_2O_2 defence [8]. Cancer cells rely on AMPK and AKT pathways to manage metabolic and ROS stresses, exert antioxidant defense, and promote cancer progression [32, 35]. AKT and AMPK can inhibit H_2O_2 accumulation by regulating the expression of antioxidant enzymes such as CAT and GPX [35]. Therefore, the expression levels of p−AKT and p–AMPK induced by H_2O_2 eustress in Caco−2 cells was examined by western blotting (Fig. 4a). It was revealed that 0.1 mmol/L H_2O_2 upregulated p−AKT, while 1 mmol/L H_2O_2 downregulated p–AKT; on the other hand, H_2O_2 upregulated AMPK in a dose−dependent manner. Since cells maintain H_2O_2 eustress via H_2O_2 scavenging enzymes, we inferred that cells regulate the expression of H_2O_2 scavenging enzymes through AKT and AMPK (Fig. 4b and c). The AKT and AMPK signaling pathway specific inhibitors were used to interrupt the pathways, and we found that H_2O_2 eustress dose–dependently increased p−AMPK levels, but inhibiting AMPK did not significantly affect the H_2O_2–induced GPX2 expression. In contrast AKT inhibition reversed the H_2O_2−induced changes in GPX2 expression. The inhibition of the AKT and AMPK pathway did not affect the expression levels of CAT in H_2O_2–treated Caco−2 cells (Fig. S10b (online)). All these experiments highlighted the critical role of the AKT pathway in fine–tuning the Caco–2 cells' response to H_2O_2 eustress through GPX2 regulation.

3.6. Involvement of F–actin dependent cellular mechanical properties in regulating AKT and AMPK signaling pathways of Caco−2 cells under H_2O_2 eustress

H_2O_2 can influence cell stiffness by targeting F−actin and actin–binding proteins, suggesting its possible impact on actin reorganization [11, 36]. The AKT and AMPK pathways are known to play critical roles in actin cytoskeleton reorganization and regulation of cellular mechanical properties [10]. To investigate the involvement of F–actin dependent cellular stiffness in regulating the activity of AKT and AMPK, we perturbed Caco−2 cellular F−actin cytoskeleton with the F–actin enhancer Jasplakinolide (Jas) or disruptor Cytochalasin D (CD) (Fig. 5). We demonstrated that Jas increased F–actin and cellular stiffness, whereas CD decreased F−actin and cellular stiffness (Fig. 5a and b). Jas upregulated p–AKT and decreased GPX2 expression, while CD resulted in decreased p−AKT and increased GPX2 expression (Fig. 5c). Neither F–actin reorganization treatments had a significant effect on AMPK activity (Fig. 5c). The effects of F−actin remodeling agents on cellular stiffness, AKT pathway activity, and GPX2 expression resemble

the responses observed under H_2O_2 eustress, indicating the involvement of F–actin dependent cellular stiffness in AKT signaling and GPX expression, which are critical for Caco−2 cells' response to H_2O_2 eustress.

3.7. The therapeutic implications of anti−H_2O_2–scavenging enzymes of GPX and/or CAT in colorectal cancer (CRC)

The higher levels of H_2O_2 in cancer cells make them more susceptible to lethality, representing their vulnerability [17]. It has been suggested that GPX primarily eliminates lower concentrations of H_2O_2, while CAT becomes more important at higher concentrations [37]. In this study, the therapeutic potential of the GPX inhibitor Tiopronin (Tiop) and/or CAT inhibitor 3−Amino–1,2,4−triazole (3AT) was explored in 1 mmol/L H_2O_2–eustress treated Caco–2 cells (Fig. 6). Morphological features associated with apoptosis, such as cell shrinkage and membrane blebbing, were observed in Tiop– and/or 3AT–treated Caco−2 cells with HPICM (Fig. 6a). Flow cytometric analysis confirmed that 1 mmol/L H_2O_2 eustress increased the apoptosis in these Tiop– and/or 3AT–treated Caco−2 cells (Fig. 6b). Cleaved caspase–3, a marker of apoptosis, was also elevated in Caco−2 cells pretreated with CAT and/or GPX inhibitors and then exposed to 1 mmol/L H_2O_2 eustress (Fig. S10c (online)). The inhibition of GPX and/or CAT in Caco–2 cells resulted in apoptosis under previous 1 mmol/L H_2O_2 eustress, indicates the therapeutic potential of targeting anti–H_2O_2−scavenging enzymes, such as GPX and/or CAT, in CRC treatment.

4. Discussion and conclusion

The phrase "what doesn't kill you makes you stronger" can be applied to short−term low–dose H_2O_2, a common environmental stressor in the gut that can be a beneficial eustress and act as signaling messenger to regulate colorectal cancer (CRC) cellular functions through still unknown mechanisms [3, 7]. Moreover, cancer cells maintain higher H_2O_2 levels than normal cells and are more susceptible to H_2O_2−targeting therapies, such as chemotherapy, radiotherapy, and photodynamic therapy [19, 32]. However, during cancer development and the process of therapy resistance, the cancer cells gradually enhance their H_2O_2 resistance [38]. Understanding how to manipulate H_2O_2 eustress in individual CRC cells can have significant implications for developing novel therapies for cancer and other H_2O_2–related inflammatory diseases [39].

The intricate relationship between reactive oxygen species (ROS), particularly H_2O_2, and the AKT pathway reveals dual regulatory roles in processes linked to cancer development, as expertly discussed by Shiau et al. [40] in a recent review on the impact of ROS and the AKT pathway. This insightful review categorizes four distinct responses to the interplay between ROS and AKT: ROS activating AKT, ROS inhibiting AKT, AKT−induced ROS generation, and AKT–mediated suppression of ROS. Specifically, a low level of H_2O_2 activates AKT, promoting cell survival [41, 42], while an overdose of H_2O_2 can inactivate AKT signaling, resulting in the inhibition of cell proliferation and the induction of apoptosis [43, 44]. Importantly, these findings align with our own observations, where AKT was upregulated in response to 0.1 mmol/L H_2O_2 but down–regulated under conditions of 1 mmol/L H_2O_2 eustress in the present study.

When epithelial cells are challenged with stresses, they tend to enhance cellular mechanical properties to maintain the integrity of the epithelial monolayer [45]. H_2O_2 stress has been demonstrated to promote actin polymerization, induce the formation of intercellular junctions, and increase the colocalization of myosin with F–actin, suggesting a role in regulating cellular mechanical properties [46]. Concurrently, studies have shown that cellular mechanical forces can regulate the PI3K/AKT signaling pathway, promoting cell proliferation, and inhibiting apoptosis [47, 48]. Observations also indicate that myotube cells become stiffer after 1 h of 0.5, 1, and 2 mmol/L H_2O_2 exposures but softer after 2 h and 24 h due to decreased F–actin polymerization in the myotubes [49]. Collectively, these studies underscore the existence of a regulatory network involving H_2O_2, mechanical properties, and the AKT signaling pathway. GPX, a crucial enzyme regulating cellular H_2O_2 levels, plays a multifaceted role in tumor proliferation and metastasis by interacting with PI3K/AKT/NRF2 signaling axis [50]. In lung cancer A549 epithelial cells, the inhibition of metastasis by 3,4−Dihydroxybenzalactone, a fungal−derived component, suppresses the PI3K/AKT signaling pathway while concurrently enhancing GPX activity [51]. Studies on non–small cell lung cancer cell lines further indicate that suppressing the PI3K/AKT pathway amplifies GPX enzyme activity [52]. All these studies suggest a potential negative correlation between AKT activity and GPX2 expression.

The extracellular to intracellular H_2O_2 gradients are a result of dynamic interactions between its production and antioxidant activity, which can be locally fine–tuned with enzymatic antioxidants, such as GPX and CAT [7, 19]. Depending on the cell types, such H_2O_2 gradients can reach an estimated 100–fold difference or even more [3, 53]. Using HPICM and its based Pt−functionalized nanoelectrode, we conducted real–time quantitative assessments of H_2O_2 gradients at the single−cell level and revealed a basal H_2O_2 gradient of approximately 0.3. When exposed to a 1 mmol/L H_2O_2 eustress producing a gradient of about 3, the increased intracellular GPX2 activity could maintain cellular H_2O_2 homeostasis by efficiently reducing the extracellular H_2O_2 level. However, at lower 0.1 mmol/L H_2O_2 eustress with a gradient of about 2, the decreased expression of GPX2 can slow down H_2O_2 detoxification, resulting in a prolonged low level of H_2O_2 eustress. We observed that both low (0.1 mmol/L) and high (1 mmol/L) levels of H_2O_2 eustress can either upregulate or downregulate F–actin polymerization, impacting cellular stiffness and subsequently modulating the AKT signaling pathway. The tuning of AKT activity further reversely regulates GPX2 expression, playing a crucial role in maintaining H_2O_2 homeostasis in Caco–2 cells. Our investigation provides new evidence indicating the negative regulation of GPX2 expression by AKT under varying levels of H_2O_2 eustress. While further investigations are warranted to delineate the detailed regulatory mechanisms between GPX2 and AKT, our current results elucidate the intricate relationship among the H_2O_2 gradients, F–actin cytoskeleton reorganization, cellular mechanical properties, AKT pathway activity, and GPX2 expression, proposing a novel mechanism for cellular H_2O_2 eustress homeostasis in CRC cells. To illustrate these homeodynamic intracellular mechanisms, we have created a schematic diagram (Fig. 7). Gaining a deeper understanding of this intricate interplay and regulation will help the development of therapeutic strategies targeting H_2O_2.

While AKT stands out as a critical regulator in defending against H_2O_2 eustress in colorectal cancer cells, the interplay between AKT and various antioxidant pathways could be pivotal in

determining the ultimate outcome in response to redox stress [8]. Our observations reveal a dose−dependent activation of several survival proteins and pathways [7], including NRF2, HSP27, MAPK, p53, STAT3, NFκB, and NOXO1, in Caco–2 cells subjected to H_2O_2 eustress (Fig. S10 (online)). Additionally, the expression of PFKP, a rate–limiting glycolysis enzyme [54], was dose–dependently upregulated by H_2O_2 eustress (Fig. S10 (online)). Notably, it has been suggested that PFKP activation is linked to a stiffer cytoskeleton [48], implying a potential coupling of cell metabolism to the observed H_2O_2−induced changes in cellular mechanical properties. Collectively, our findings suggest that the activities of AKT, AMPK, PFKP, and other pathways mentioned encompass antioxidant defense mechanisms and metabolic changes. These orchestrated responses enable individual CRC cells to harness H_2O_2 eustress as an advantage for optimizing survival and growth.

Our observations may explain the failure of some H_2O_2 targeting therapies not only due to ineffective generation of H_2O_2 but also because they act as eustress to promote survival of cancer cells [3, 5]. Our findings demonstrate that interfering with antioxidative systems, specifically inhibition of GPX and/or CAT, enhances the cytotoxic activity of H_2O_2 eustress against CRC cells. Overexpression or targeted delivery of H_2O_2 scavenging enzymes, such as CAT or GPX, has been shown to inhibit metastatic tumor growth and reverse the malignant phenotype [55]. Combination therapies involving radiotherapy, chemotherapy, and immune checkpoint inhibitors along with GPX inhibitors have demonstrated promise in preclinical studies and animal models [56]. In particular, the inhibition of antioxidant enzymes such as GPX2 holds significant promise for patients undergoing H_2O_2–inducing chemoradiotherapies [57], and has the potential to enhance therapeutic outcomes of CRC treatment.

In addition to CRC, H_2O_2 eustress also leads to the development of other intestinal pathological conditions such as inflammatory bowel disease and ischemic−reperfusion injury [58]. Intestinal microbes can exploit colonic epithelium produced H_2O_2 for a growth advantage during both normal and inflammatory conditions [58]. More interestingly, new research suggests that the death observed in sleep–deprived animals can be attributed to the accumulation of H_2O_2 in the gut, and it has been demonstrated that preventing gut H_2O_2 accumulation can enable survival in the absence of sleep [59]. Our observed cellular stiffness dependent self–adaptive ability to facilitate H_2O_2 eustress will enhance the knowledge of H_2O_2 signaling and, hopefully, could lead to the development of more refined redox therapies for CRC and other H_2O_2 related diseases.

Acknowledgements
This work was supported by Japan Society for the Promotion of Science KAKENHI Grants 21H01770, 22K04890, and World Premier International Research Center Initiative (WPI), MEXT, Japan.

Additional Information
Supplementary information is available in the online version of the paper. Reprints and permission information is available online at www.nature.com/reprints. Correspondence and requests for materials should be addressed to the corresponding author.

Data Availability
The data that support the plots within this paper and other findings of this study are available from the corresponding author upon reasonable request.

Competing interests
Christopher Edwards and Yuri Korchev are shareholders in ICAPPIC Ltd, a company commercialising nanopipette–based instrumentation. All other authors declare no competing interests.

Author contributions
Yanjun Zhang, Yuri Korchev, Elena V Sviderskaya designed and supervised the research. Yanjun Zhang, Dong Wang, Xi Yang, Emily Woodcock performed the experiments and analysed the data. Hiromi Nishikawa, Emily Woodcock prepared the cell samples. Yanjun Zhang, Dong Wang, Masanobu Oshima, Christopher Edwards, Yuri Korchev prepared the manuscript. All the authors discussed the results and commented on the manuscript.

Fig.1

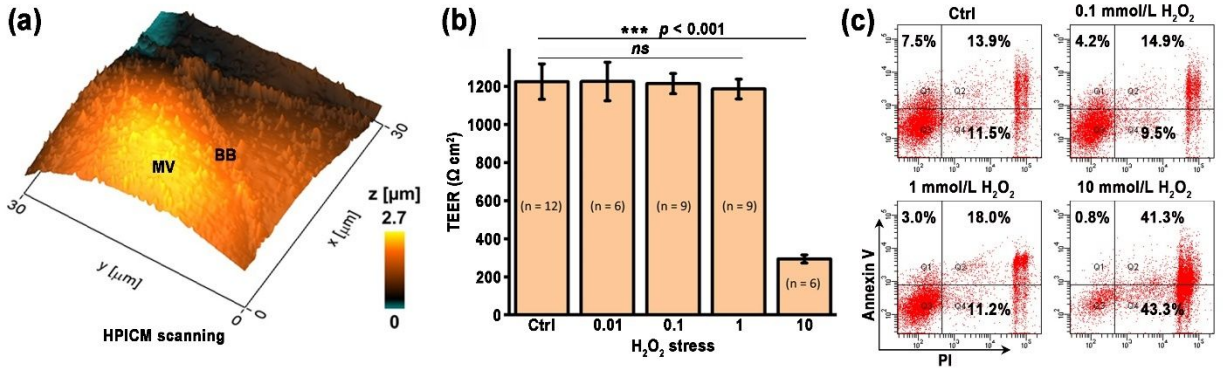

Fig. 1. Determination of acute exogenous H_2O_2 eustress levels in colorectal cancer Caco−2 cells. (a) Hopping Probe Mode Scanning Ion Conductance Microscopy (HPICM) was employed to scan the Caco–2 cell monolayer, clearly delineating the structures of the brush border (BB) and microvilli (MV) as marked in the 3D HPICM scanning image; (b) The impact of varying H_2O_2 concentrations on the TEER of Caco–2 cell monolayers. Data are presented as mean ± SEM of replicates. Statistical differences between the H_2O_2–treated cell monolayers and the control were determined by Student *t*–test. *** $p < 0.001$, ns $p > 0.05$; (c) Flow cytometric analysis on Caco−2 cells exposed to varied extracellular H_2O_2 concentrations for 2 h using Annexin V/PI early apoptosis detection kit.

Fig.2

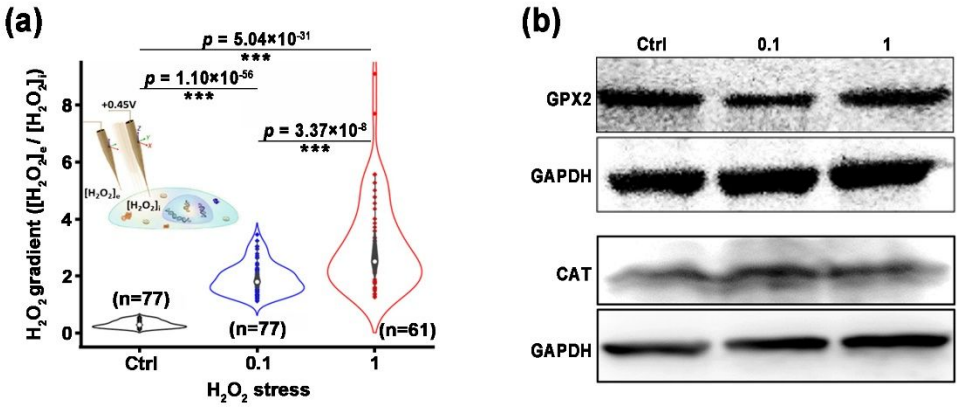

Fig. 2. Investigation responses of individual Caco–2 cells to H_2O_2 eustress with hopping probe mode scanning ion conductance microscopy (HPICM) combined Pt–functionalized carbon nanoelectrodes and western blot analysis. (a) Violin plots for H_2O_2 gradients of individual Caco−2 cells in each condition group under varying levels of H_2O_2 eustress. Markers with error bars indicate median ± interquartile range. The number of cells is shown in parentheses for each group. *P* values were calculated using the student *t* test. The average H_2O_2 gradients in the cells under H_2O_2 eustress were increased from 0.3 ± 0.13 (n = 77, control), to 1.91 ± 0.54 (n = 77, 0.1 mmol/L–treated), and 3.04 ± 1.58 (n = 61, 1 mmol/L–treated), respectively. The conceptual image embedded illustrates the dynamic detection of both extracellular and intracellular H_2O_2 concentrations at + 0.45 V. This detection is facilitated by Pt−functionalized carbon nanoprobes, meticulously controlled through HPICM operating as a scanning electrochemical microscope. (b) Western blot analysis of the expression of two major H_2O_2 scavenging enzymes catalase (CAT) and glutathione peroxidase 2 (GPX2) in Caco–2 cells under 0.1 or 1 mmol/L H_2O_2 eustress.

Fig.3

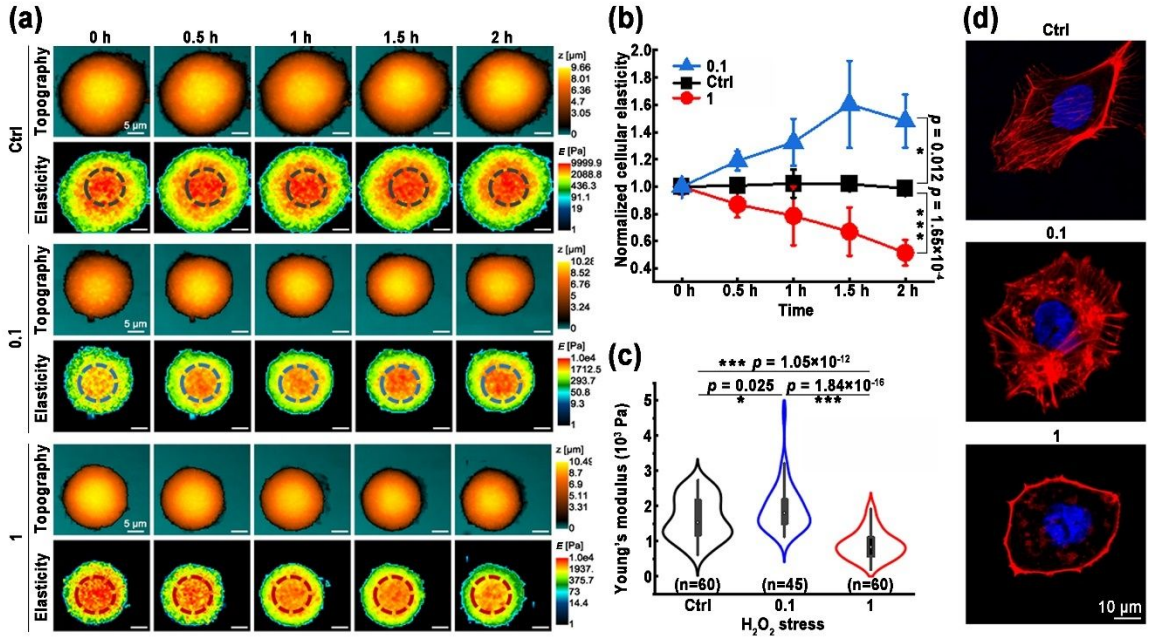

Fig. 3. Investigation of the F−actin dependent mechanical properties response of individual Caco−2 cells to H_2O_2 eustress with hopping probe mode scanning ion conductance microscopy (HPICM) and confocal microscopy. (a) The effects of H_2O_2 eustress on cellular mechanical properties of individual Caco–2 cells were investigated with HPICM scanning. Six images selected from a series of 2 h time–lapse HPICM scans of a living Caco−2 cell exposed to different levels of H_2O_2 eustress from the time 0 h. (b) The normalized mean profile of cellular elasticity changes in response to a 2 h H_2O_2 eustress was determined by calculating the average values derived from three separate replicates of H_2O_2–treated individual Caco−2 cells. Error bars represent the standard error of the mean. (c) Violin plots for Young's Modulus of individual Caco–2 cells in each condition group under varying levels of H_2O_2 eustress. Markers with error bars indicate median ± interquartile range. The number of cells is shown in parentheses for each group. *P* values were calculated using the student *t* test. (d) Confocal microscopy images of actin filaments labeling with phalloidin (red) and DAPI (blue) of individual Caco−2 cells under varying levels of H_2O_2–eustress.

Fig.4

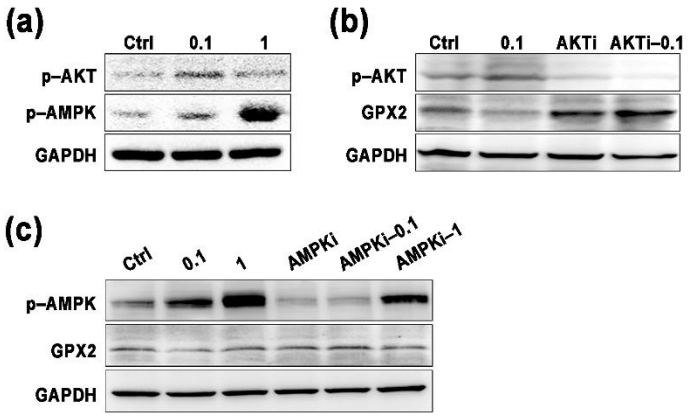

Fig. 4. Western blot analysis of antioxidant–related protein expression in Caco−2 cells under varying levels of H_2O_2 eustress without (a) or with AKT (b) and AMPK inhibition (c). The protein expressions of p–AKT, p−AMPK, and GPX2 were evaluated using western blotting.

Fig.5

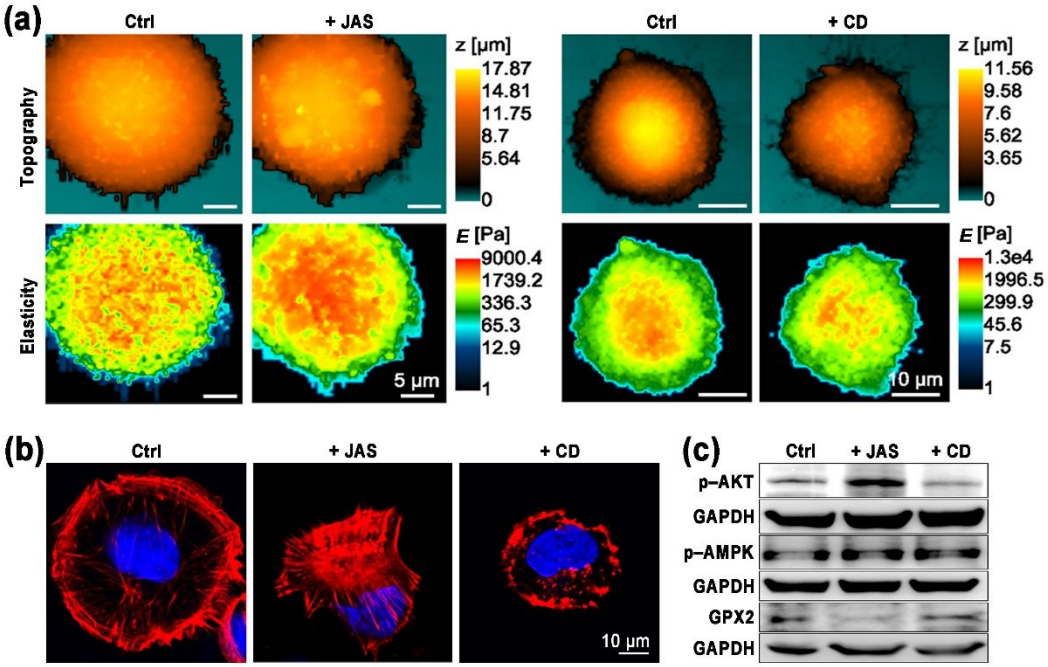

Fig. 5. The effects of 2 h F–actin targeting enhancer Jasplakinolide (JAS) or disruptor Cytochalasin D (CD) treatment on Caco−2 cells topography and mechanical properties were observed with HPICM (a). F−actin cytoskeleton was labeled with phalloidin and observed with confocal microscopy (b). The protein expressions of p–AKT, p−AMPK, and GPX2 in JAS or CD treated Caco–2 cells were assessed by western blot analysis (c).

Fig.6

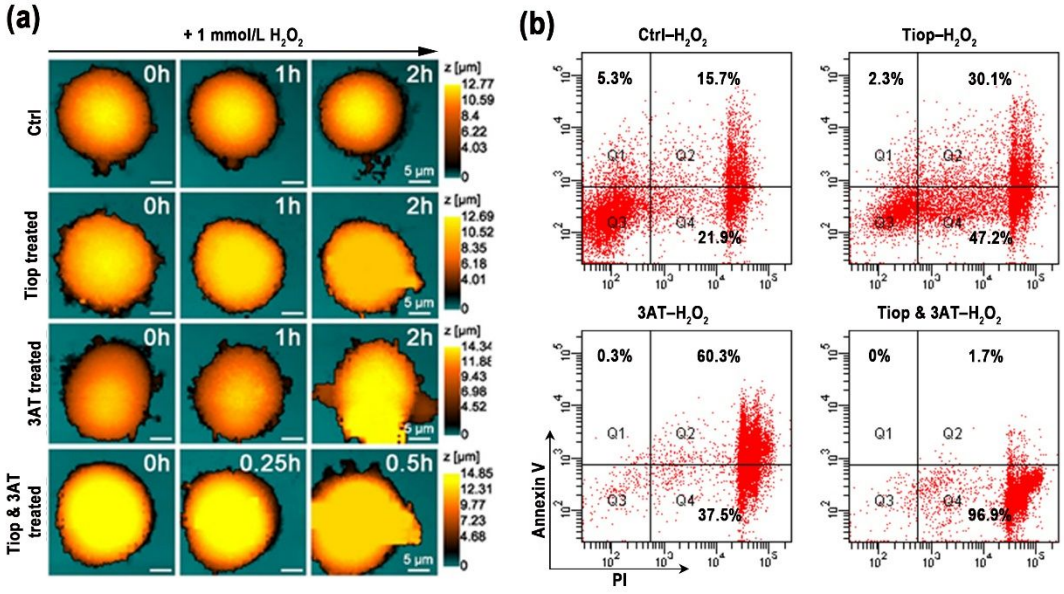

Fig. 6. Under 1 mmol/L H_2O_2 eustress, inhibiting GPX and/or CAT, key anti–H_2O_2–scavenging enzymes, induced apoptosis in colorectal cancer Caco–2 cells. (a) HPICM time–lapse scannings were conducted to examine cellular morphology changes induced by 1 mmol/L H_2O_2 eustress in Caco–2 cells treated with GPX inhibitor Tiopronin (Tiop) and/or CAT inhibitor 3–Amino–1,2,4–triazole (3AT). (b) Flow cytometric analysis was conducted to evaluate apoptosis in Caco–2 cells treated with Tiop and/or 3AT, exposed to 1 mmol/L H_2O_2 eustress for 2 h, using the Annexin V/PI early apoptosis detection kit.

Fig.7

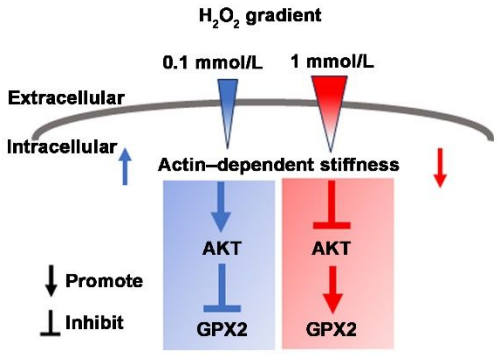

Fig. 7. Schematic diagram shows the response mechanisms of individual colorectal cancer cells to H_2O_2 eustress.

References

[1] La Vecchia S, Sebastian C. Metabolic pathways regulating colorectal cancer initiation and progression. Semin Cell Dev Biol, 2020, 98: 63–70

[2] Mittal M, Siddiqui MR, Tran K, et al. Reactive oxygen species in inflammation and tissue injury. Antioxid Redox Signal, 2014, 20: 1126–1167

[3] Sies H. Oxidative eustress: On constant alert for redox homeostasis. Redox Biol, 2021, 41: 101867

[4] Pérez S, Taléns-Visconti R, Rius-Pérez S, et al. Redox signaling in the gastrointestinal tract. Free Radic Bio Med, 2017, 104: 75–103

[5] Herb M, Gluschko A, Schramm M. Reactive oxygen species: Not omnipresent but important in many locations. Front Cell Dev Biol, 2021, 9: 716406

[6] Raza MH, Siraj S, Arshad A, et al. Ros–modulated therapeutic approaches in cancer treatment. J Cancer Res Clin Oncol, 2017, 143: 1789–1809

[7] Liao ZH, Chua D, Tan NS. Reactive oxygen species: A volatile driver of field cancerization and metastasis. Mol Cancer, 2019, 18: 65

[8] Cheung EC, Vousden KH. The role of ROS in tumour development and progression. Nat Rev Cancer, 2022, 22: 280–297

[9] Evers TMJ, Holt LJ, Alberti S, et al. Reciprocal regulation of cellular mechanics and metabolism. Nat Metab, 2021, 3: 456–468

[10] Ge HM, Tian MX, Pei Q, et al. Extracellular matrix stiffness: New areas affecting cell metabolism. Front Oncol, 2021, 11: 631991

[11] Ishimoto T, Mori H. Control of actin polymerization via reactive oxygen species generation using light or radiation. Front Cell Dev Biol, 2022, 10: 1014008

[12] Novak P, Li C, Shevchuk AI, et al. Nanoscale live–cell imaging using hopping probe ion conductance microscopy. Nat Methods, 2009, 6: 279–281

[13] Kolmogorov VS, Erofeev AS, Woodcock E, et al. Mapping mechanical properties of living cells at nanoscale using intrinsic nanopipette–sample force interactions. Nanoscale, 2021, 13: 6558–6568

[14] Woodcock E, Gorelkin PV, Goff PS, et al. Measuring melanoma nanomechanical properties in relation to metastatic ability and anti–cancer drug treatment using scanning ion conductance microscopy. Cells, 2023, 12: 2401

[15] Seifert J, Rheinlaender J, Novak P, et al. Comparison of atomic force microscopy and scanning ion conductance microscopy for live cell imaging. Langmuir, 2015, 31: 6807–6813

[16] Hosogi S, Marunaka Y, Ashihara E, et al. Plasma membrane anchored nanosensor for quantifying endogenous production of H_2O_2 in living cells. Biosens Bioelectron, 2021, 179: 113077

[17] Di Filippo ES, Checcaglini F, Fanò-Illic G, et al. H_2O_2/ca^{2+}/zn^{2+} complex can be considered a "collaborative sensor" of the mitochondrial capacity? Antioxidants (Basel), 2022, 11: 342

[18] Carmona M, de Cubas L, Bautista E, et al. Monitoring cytosolic H_2O_2 fluctuations arising from altered plasma membrane gradients or from mitochondrial activity. Nat Commun, 2019, 10: 4526

[19] Sies H. Hydrogen peroxide as a central redox signaling molecule in physiological oxidative stress: Oxidative eustress. Redox Biol, 2017, 11: 613–619

[20] Winterbourn CC. The biological chemistry of hydrogen peroxide. Methods Enzymol, 2013, 528: 3–25

[21] Actis P, Tokar S, Clausmeyer J, et al. Electrochemical nanoprobes for single–cell analysis. ACS Nano, 2014, 8: 875–884

[22] Vaneev AN, Gorelkin PV, Garanina AS, et al. In vitro and in vivo electrochemical measurement of reactive oxygen species after treatment with anticancer drugs. Anal Chem, 2020, 92: 8010–8014

[23] Hu KK, Li Y, Rotenberg SA, et al. Electrochemical measurements of reactive oxygen and nitrogen species inside single phagolysosomes of living macrophages. J Am Chem Soc, 2019, 141: 4564–4568

[24] Guardamagna I, Lonati L, Savio M, et al. An integrated analysis of the response of colorectal adenocarcinoma Caco–2 cells to x–ray exposure. Front Oncol, 2021, 11: 688919

[25] Wang D, Sun LH, Okuda S, et al. Nano–scale physical properties characteristic to metastatic intestinal cancer cells identified by high–speed scanning ion conductance microscope. Biomaterials, 2022, 280: 121256

[26] Zhang YJ, Gorelik J, Sanchez D, et al. Scanning ion conductance microscopy reveals how a functional renal epithelial monolayer maintains its integrity. Kidney Int, 2005, 68: 1071–1077

[27] Zhang YJ, Takahashi Y, Hong SP, et al. High–resolution label–free 3D mapping of extracellular pH of single living cells. Nat Commun, 2019, 10: 5610

[28] Lyublinskaya OG, Ivanova JS, Pugovkina NA, et al. Redox environment in stem and differentiated cells: A quantitative approach. Redox Biol, 2017, 12: 758–769

[29] Buckley CE, St Johnston D. Apical–basal polarity and the control of epithelial form and function. Nat Rev Mol Cell Biol, 2022, 23: 559–577

[30] Redondo PAG, Nakamura CV, de Souza W, et al. Differential expression of sialic acid and n–acetylgalactosamine residues on the cell surface of intestinal epithelial cells according to normal or metastatic potential. J Histochem Cytochem, 2004, 52: 629–640

[31] Antunes F, Cadenas E. Estimation of H_2O_2 gradients across biomembranes. FEBS Lett, 2000, 475: 121–126

[32] Zhao Y, Hu XB, Liu YJ, et al. ROS signaling under metabolic stress: Cross–talk between AMPK and AKT pathway. Mol Cancer, 2017, 16: 79

[33] Hall MD, Marshall TS, Kwit ADT, et al. Inhibition of glutathione peroxidase mediates the collateral sensitivity of multidrug–resistant cells to tiopronin. J Biol Chem, 2014, 289: 21473–21489

[34] Doss BL, Pan M, Gupta M, et al. Cell response to substrate rigidity is regulated by active and passive cytoskeletal stress. Proc Natl Acad Sci U S A, 2020, 117: 12817–12825

[35] Hoxhaj G, Manning BD. The PI3K–AKT network at the interface of oncogenic signalling and cancer metabolism. Nat Rev Cancer, 2020, 20: 74–88

[36] Chugh P, Clark AG, Smith MB, et al. Actin cortex architecture regulates cell surface tension. Nat Cell Biol, 2017, 19: 689–697

[37] Campbell EL, Colgan SP. Control and dysregulation of redox signalling in the gastrointestinal tract. Nat Rev Gastroenterol Hepatol, 2019, 16: 106–120

[38] Huang G, Pan ST. ROS–mediated therapeutic strategy in chemo–/radiotherapy of head and neck cancer. Oxid Med Cell Longev, 2020, 2020: 5047987

[39] Weinberg F, Ramnath N, Nagrath D. Reactive oxygen species in the tumor microenvironment: An overview. Cancers (Basel), 2019, 11: 1191

[40] Shiau JP, Chuang YT, Tang JY, et al. The impact of oxidative stress and AKT pathway on cancer cell functions and its application to natural products. Antioxidants (Basel), 2022, 11: 1845

[41] Sadidi M, Lentz SI, Feldman EL. Hydrogen peroxide–induced Akt phosphorylation regulates Bax activation. Biochimie, 2009, 91: 577–585

[42] Park JH, Kim CK, Lee SB, et al. Akt attenuates apoptotic death through phosphorylation of H_2A under hydrogen peroxide–induced oxidative stress in PC12 cells and hippocampal neurons. Sci Rep, 2016, 6: 21857

[43] Wang FJ, Wang L, Qu C, et al. Kaempferol induces ROS–dependent apoptosis in pancreatic cancer cells via TGM2–mediated Akt/mTOR signaling. BMC Cancer, 2021, 21: 396

[44] Pang H, Wu TR, Peng ZH, et al. Baicalin induces apoptosis and autophagy in human osteosarcoma cells by increasing ROS to inhibit PI3K/Akt/mTOR, ERK1/2 and beta–catenin signaling pathways. J Bone Oncol, 2022, 33: 100415

[45] Liu ZJ, Tan JL, Cohen DM, et al. Mechanical tugging force regulates the size of cell–cell junctions. Proc Natl Acad Sci U S A, 2010, 107: 9944–9949

[46] Zhu DH, Tan KS, Zhang XL, et al. Hydrogen peroxide alters membrane and cytoskeleton properties and increases intercellular connections in astrocytes. J Cell Sci, 2005, 118: 3695–3703

[47] Da Y, Mou YB, Wang MJ, et al. Mechanical stress promotes biological functions of C2C12 myoblasts by activating PI3K/AKT/mTOR signaling pathway. Mol Med Rep, 2020, 21: 470–477

[48] De Belly H, Paluch EK, Chalut KJ. Interplay between mechanics and signalling in regulating cell fate. Nat Rev Mol Cell Biol, 2022, 23: 465–480

[49] Wong SW, Sun S, Cho M, et al. H_2O_2 exposure affects myotube stiffness and actin filament polymerization. Ann Biomed Eng, 2015, 43: 1178–1188

[50] Koundouros N, Poulogiannis G. Phosphoinositide 3–kinase/Akt signaling and redox metabolism in cancer. Front Oncol, 2018, 8: 160

[51] Chao W, Deng JS, Li PY, et al. 3,4–dihydroxybenzalactone suppresses human non–small cell lung carcinoma cells metastasis via suppression of epithelial to mesenchymal transition, ROS–mediated PI3K/AKT/MAPK/MMP and NFκB signaling pathways. Molecules, 2017, 22: 537

[52] Akca H, Demiray A, Aslan M, et al. Tumour suppressor PTEN enhanced enzyme activity of GPx, SOD and catalase by suppression of PI3K/AKT pathway in non–small cell lung cancer cell lines. J Enzyme Inhib Med Chem, 2013, 28: 539–544

[53] Domènech A, Ayté J, Antunes F, et al. Using in vivo oxidation status of one– and two–component redox relays to determine H_2O_2 levels linked to signaling and toxicity. BMC Biol, 2018, 16: 61

[54] Lang LW, Chemmalakuzhy R, Shay C, et al. PFKP signaling at a glance: An emerging mediator of cancer cell metabolism. Adv Exp Med Biol, 2019, 1134: 243–258

[55] Trachootham D, Alexandre J, Huang P. Targeting cancer cells by ROS–mediated mechanisms: A radical therapeutic approach? Nat Rev Drug Discov, 2009, 8: 579–591

[56] Nimalasena S, Gothard L, Anbalagan S, et al. Intratumoral hydrogen peroxide with radiation therapy in locally advanced breast cancer: Results from a phase 1 clinical trial. Int J Radia Oncol Biol Phys, 2020, 108: 1019–1029

[57] Wang M, Chen X, Fu G, et al. Glutathione peroxidase 2 overexpression promotes malignant progression and cisplatin resistance of KRAS–mutated lung cancer cells. Oncol Rep, 2022, 48: 207

[58] Crowley SM, Vallance BA. Microbial respiration in the colon: Using H_2O_2 to catch your breath. Cell Host Microbe, 2020, 28: 771–773

[59] Vaccaro A, Dor YK, Nambara K, et al. Sleep loss can cause death through accumulation of reactive oxygen species in the gut. Cell, 2020, 181: 1307–1328

Dr. Dong Wang earned his doctoral degree from the University of Science and Technology of China. He currently holds the position of assistant professor at Kanazawa University in Japan, where his primary research involves utilizing scanning probe technology to explore the occurrence and development processes of tumor cells.

Dr. Yanjun Zhang, Associate Professor at WPI Nano LSI, Kanazawa University, Japan, and Honorary Senior Research Fellow at Imperial College London, UK. He earned his Ph.D. from Imperial College London in 2005. His research focuses on non-contact scanning ion conductance microscopy (SICM) and its based nanoprobe biosensors for real-time, high-resolution detection of cellular microstructures, biomechanics, and physiological functions at single-cell and subcellular levels.

Dr. Yuri Korchev is a Professor of Biophysics at the Faculty of Medicine, Imperial College London in UK, and serves as an overseas Principal Investigator at the WPI Nano LSI in Japan. His research interests encompass SICM for precise imaging of living cells, both independently and in conjunction with nanopipette biosensors, patch clamp, and Scanning Electrochemical Microscopy for functional imaging at both the single-cell and subcellular levels.

Supplementary information for

Exploration of individual colorectal cancer cell responses to H_2O_2 eustress using hopping probe scanning ion conductance microscopy

Dong Wang[1], Emily Woodcock[2,3], Xi Yang[1], Hiromi Nishikawa[1], Elena V Sviderskaya[3], Masanobu Oshima[1], Christopher Edwards[2], Yanjun Zhang[1,2,*] , Yuri Korchev[2,1,*]

[1]WPI Nano Life Science Institute (WPI–Nano LSI), Kanazawa University, Kanazawa 920–1192, Japan;
[2]Department of Medicine, Imperial College London, London W12 0NN, United Kingdom;
[3]Cell Biology Research Centre, Molecular and Clinical Sciences Research Institute, St George's, University of London, London SW17 0RE, United Kingdom.

***Corresponding authors**: yanjunzhang@staff.kanazawa–u.ac.jp, y.korchev@imperial.ac.uk

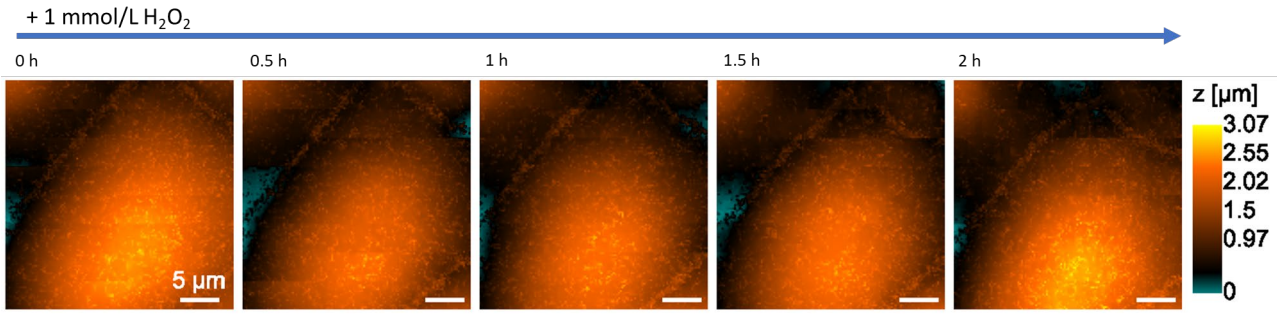

Fig. S1. 2–hour time–lapse hopping probe mode scanning ion conductance microscopy (HPICM) topographical scanning of Caco–2 cells monolayer under 1 mmol/L H_2O_2 eustress.

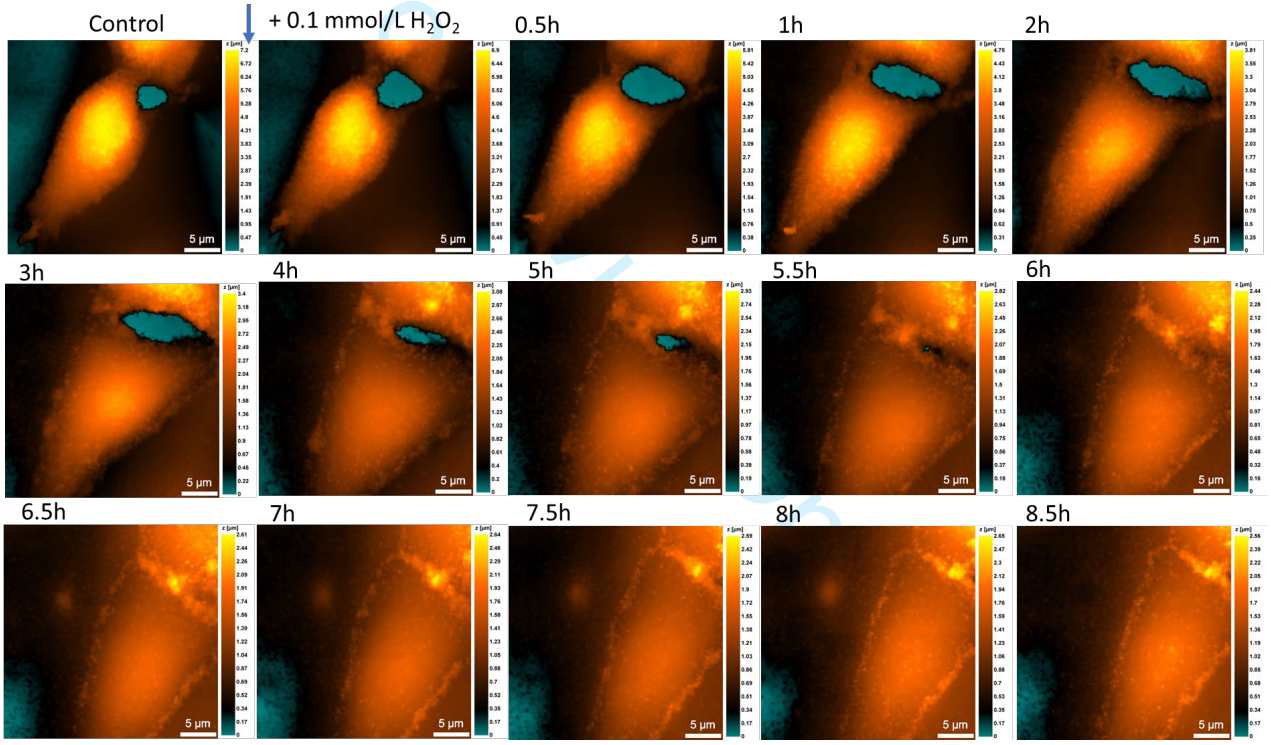

Fig. S2. 8.5–hour time–lapse HPICM topographical scanning of the formation of Caco–2 cells monolayer under 0.1 mmol/L H_2O_2 eustress.

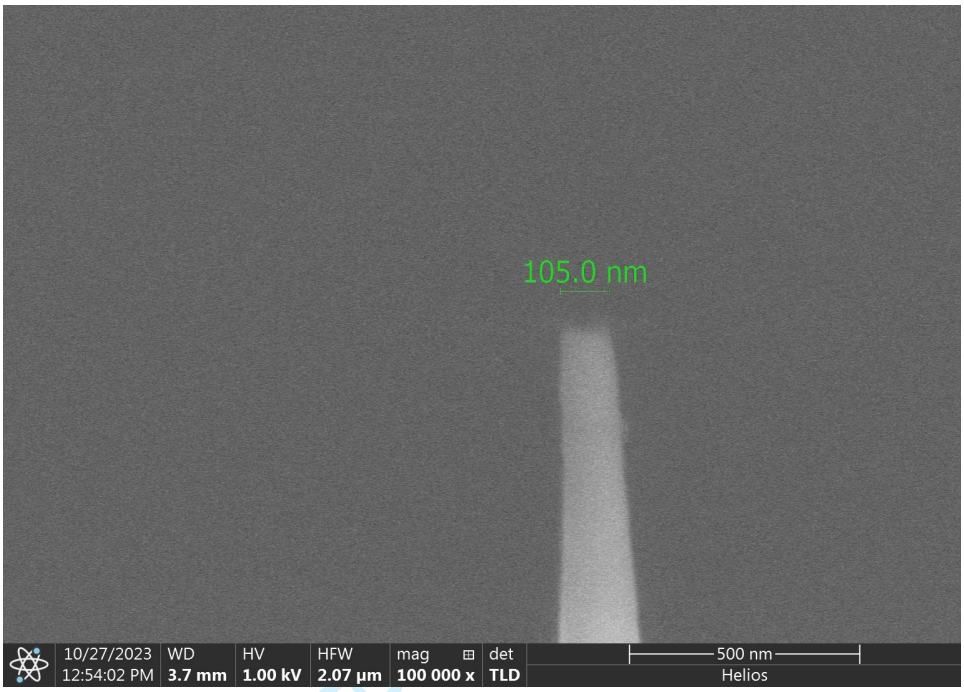

Fig. S3. SEM image of HPICM scanning nanopipette.

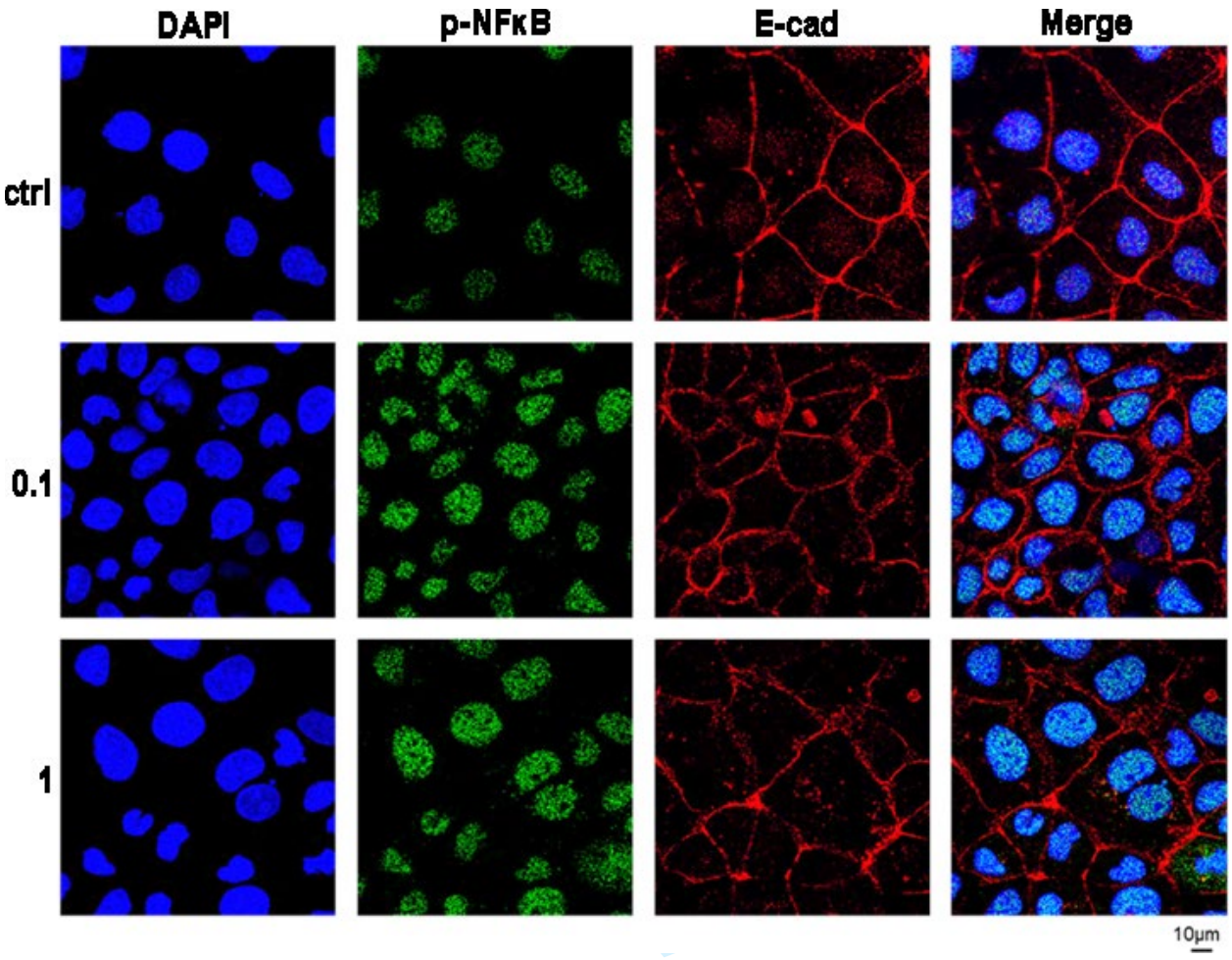

Fig. S4. H_2O_2 eustress (0.1 and 1 mmol/L) regulated expression of p–NFκB and E–cadherin (E–cad) was examined by fluorescent immunohistochemistry with confocal microscopy. p65–NFκB (green), E–cad (red), DAPI (blue).

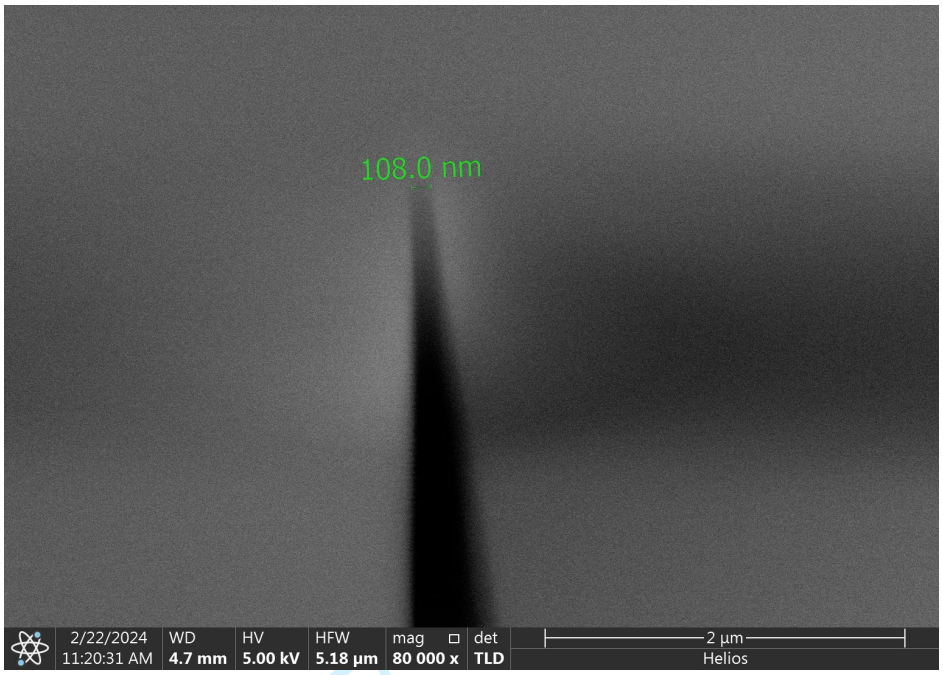

Fig. S5. SEM image of Pt–functionalized carbon nanoelectrode.

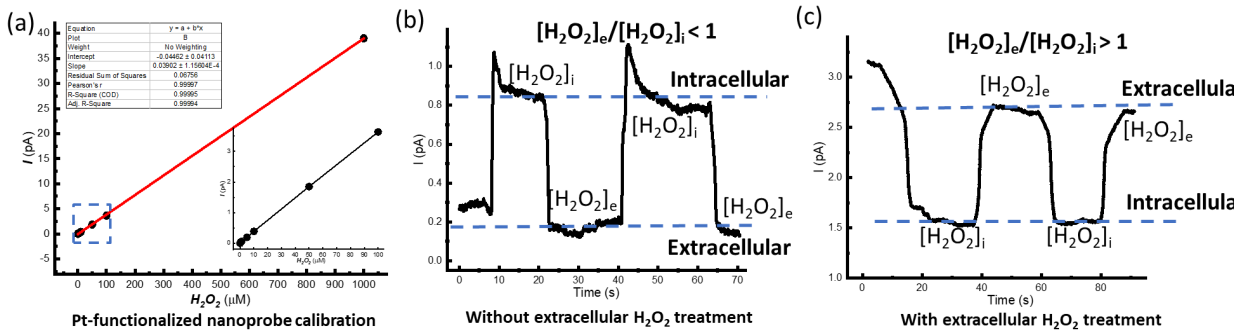

Fig. S6. HPICM–based Pt–functionalized nanoelectrode for extracellular to intracellular H_2O_2 gradients detecting at 0.45 V. (a) Standard calibration curve for quantitation of H_2O_2 with Pt-functionalized nanoelectrodes. It exhibits a remarkably linear fit, with an R^2 value of 0.9994. The inset highlights the nanoelectrode's sensitivity and linearity at low H_2O_2 levels, including concentrations of 0.5, 1, 5, 10, 50, and 100 μmol/L. (b) The repetitive extracellular to intracellular H_2O_2 gradient detecting from the same Caco–2 cell under control condition. (c) The repetitive extracellular to intracellular H_2O_2 gradient detecting from the same Caco–2 cell under 0.1 mmol/L H_2O_2 eustress.

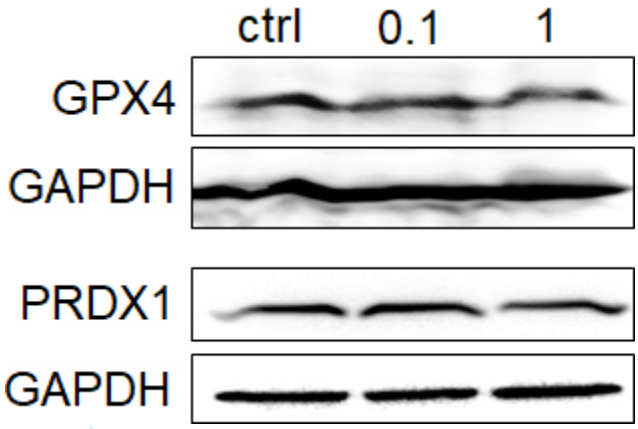

Fig. S7. Western blot analysis of the expression of H_2O_2 scavenging glutathione peroxidase GPX4 and peroxiredoxin PRDX1 in Caco–2 cells under varying levels of H_2O_2 eustress. The expressions of PRDX1 and GPX4 did not exhibit dose dependency in response to 0.1 and 1 mmol/L H_2O_2 eustress.

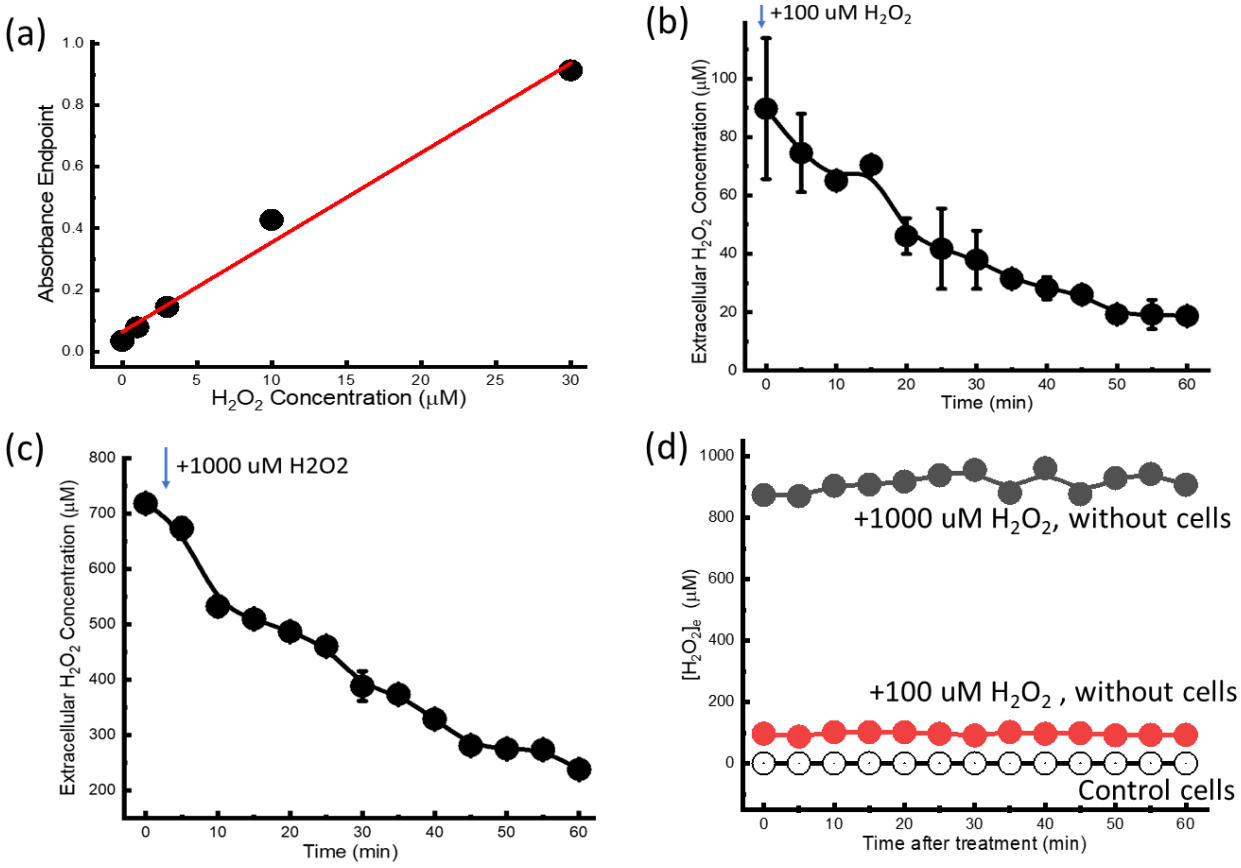

Fig. S8. Assessing the defense capacities of Caco–2 cells against H_2O_2 eustress with an Amplex Red Hydrogen Peroxide/Peroxidase Assay. (a) Standard calibration curve for quantitation of H_2O_2 with Amplex Red Hydrogen Peroxide/Peroxidase Assay; The dynamical decomposition of extracellular H_2O_2 by Caco–2 cells under 0.1 mmol/L (b) and 1 mmol/L (c) H_2O_2 eustress; (d) No decomposition when 0.1 and 1 mmol/L H_2O_2 were added to control dish without cells; No extracellular H_2O_2 level changing in control cells. All cells are cultured for 3 days at a density of 1×10^6 cells / cm^2 into 35 mm Petri dish. The H_2O_2 standard curve validates the assay's precision within a defined range of 1 to 30 μmol/L. To extend its applicability beyond this range, supernatant samples are intentionally diluted, either 5 or 40 times, for extracellular treated H_2O_2 concentrations of 0.1 or 1 mmol/L, respectively. This deliberate dilution strategy ensures that all samples remain within the linear detection capacity of the assay, thereby upholding the precision and reliability of our measurements.

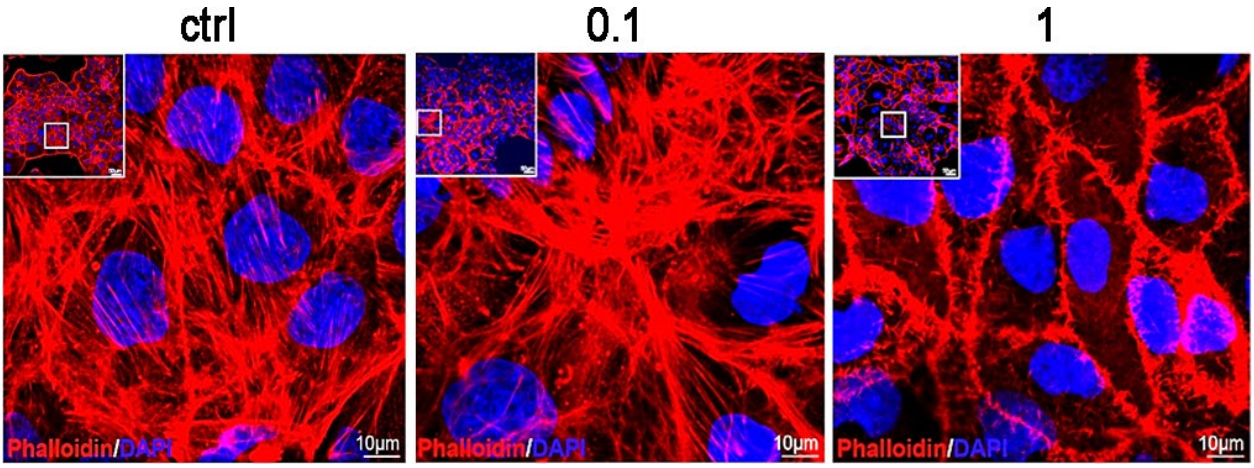

Fig. S9. Confocal microscopy images of actin filaments labeling with phalloidin (red) and DAPI (blue) of Caco–2 cells monolayers under 0.1 and 1 mmol/L H_2O_2 eustress.

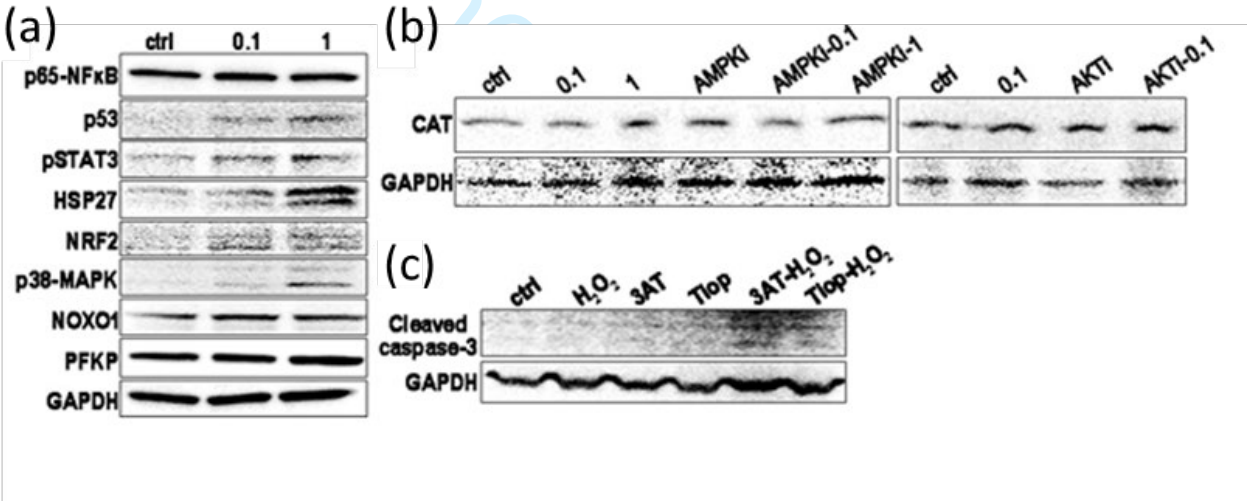

Fig. S10. Western blot analysis was conducted to evaluate the protein expression in Caco–2 cells under varying levels of H_2O_2 eustress. (a) Western blot analysis was conducted to assess the expression of well–established antioxidant defense proteins in Caco–2 cells subjected to different levels of H_2O_2 eustress. (b) Western blot analysis was performed to examine the expression of catalase (CAT) in Caco-2 cells exposed to varying levels of H_2O_2 eustress with or without the inhibition of AMPK (AMPKi) and AKT (AKTi). (c) Western blot analysis was performed to evaluate the expression of cleaved caspase-3 in control Caco–2 cells as well as those treated with the CAT inhibitor 3–Amino–1,2,4–triazole (3AT) and the GPX inhibitor Tiopronin (Tiop), both with and without a 2–h exposure to 1 mmol/L H_2O_2 eustress.

Fig.1

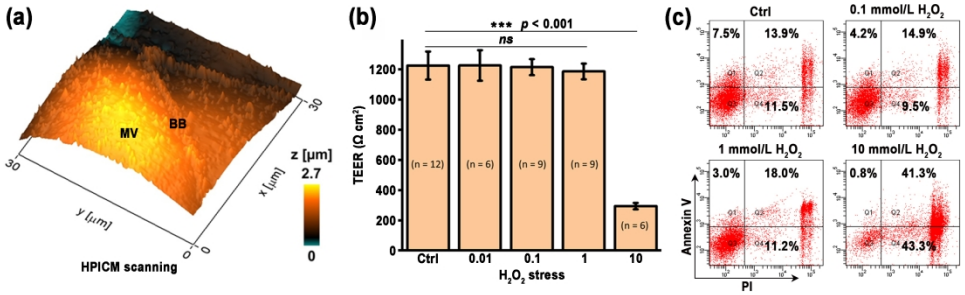

Fig.1

1237x874mm (72 x 72 DPI)

Fig.2

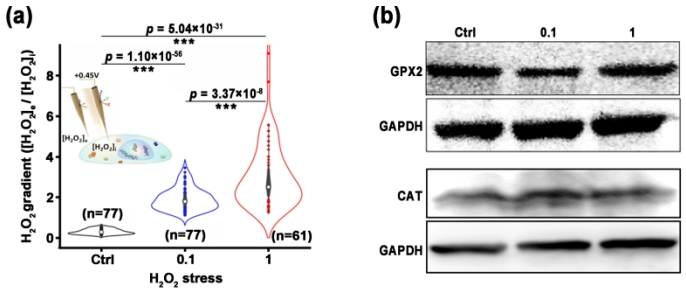

Fig. 2

1237x874mm (72 x 72 DPI)

Fig.3

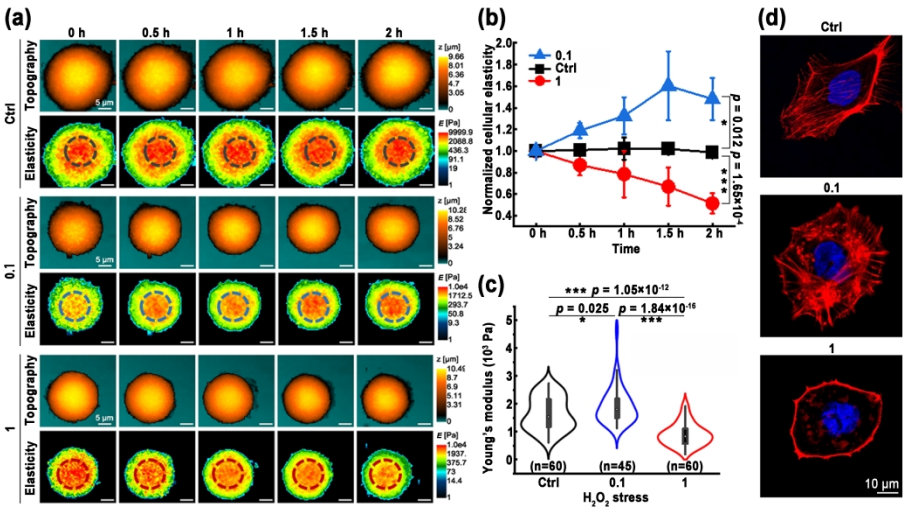

Fig. 3

1237x874mm (72 x 72 DPI)

Fig.4

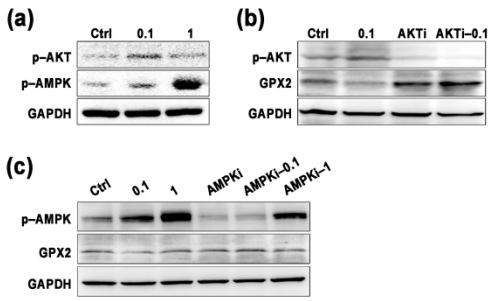

Fig. 4

1237x874mm (72 x 72 DPI)

Fig.5

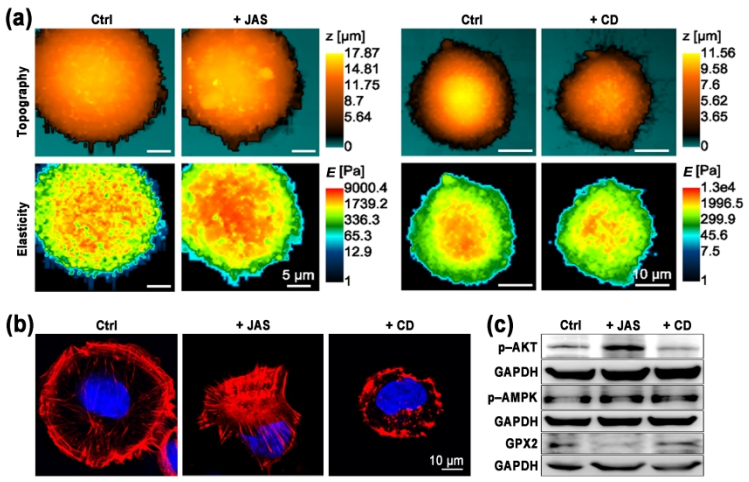

Fig. 5

1237x874mm (72 x 72 DPI)

Fig.6

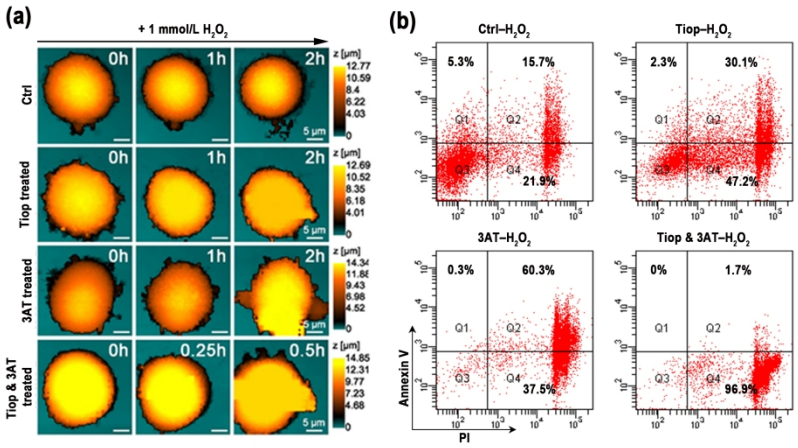

Fig. 6

1237x874mm (72 x 72 DPI)

Fig.7

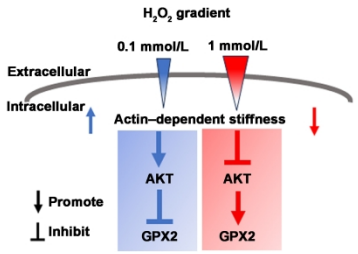

Fig. 7

1237x874mm (72 x 72 DPI)

Graphical abstract

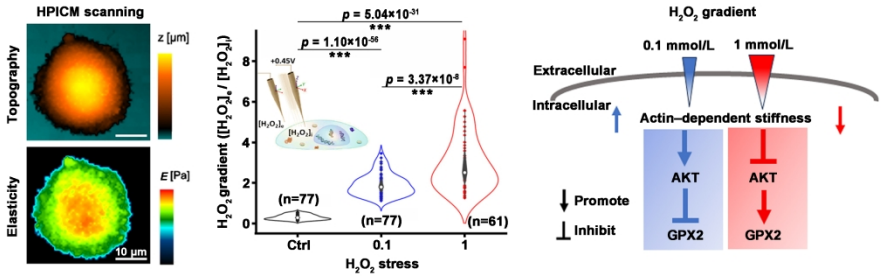

graphical abstract

1237x874mm (72 x 72 DPI)